



Genesis of carbonatite and associated U–Nb–REE mineralization at Huayangchuan, central China: Insights from mineral paragenesis, chemical and Sr–Nd–C–O isotopic compositons of calcite



Long-Gang Gao^{a,b}, You-Wei Chen^{a,*}, Xian-Wu Bi^a, Jian-Feng Gao^a, Wei Terry Chen^a, Shao-Hua Dong^a, Jin-Cheng Luo^a, Rui-Zhong Hu^{a,b,*}

^a State Key Laboratory of Ore Deposit Geochemistry, Institute of Geochemistry, Chinese Academy of Sciences, Guiyang 550081, China

^b College of Earth and Planetary Sciences, University of Chinese Academy of Sciences, Beijing 100049, China

ARTICLE INFO

Keywords:

Carbonatite genesis and evolution
U–Nb–REE mineralization
Calcite mineral chemistry
Sr–Nd–C–O isotopes
Huayangchuan deposit
Qinling orogen

ABSTRACT

The Huayangchuan deposit in the North Qinling alkaline province of Central China is a unique carbonatite-hosted giant U–Nb–REE polymetallic deposit. The mineralization is characterized by the presence of betafite, monazite, and allanite as the main ore minerals, but also exhibit relatively high budgets of heavy rare earth elements (HREE = Gd–Lu and Y). The origin of carbonatites has long been controversial, thus hindering our understanding of the genesis of the deposit. Here, we conducted an in-situ trace elemental, Sr–Nd isotopic, and bulk C–O isotopic analyses of multi-type calcites in the deposit. Two principal types (Cal-I and Cal-II), including three sub-types (Cal-I-1, Cal-I-2 and Cal-I-3) of calcites were identified based on crosscutting relationships and calcite textures. Texturally, Cal-I calcites in carbonatites display cumulates with the grain size decreasing from early coarse- (Cal-I-1) to medium- (Cal-I-2) and late fine-grained (Cal-I-3), whereas Cal-II calcites coexist with zeolite displaying zeolite–calcite veinlets. Geochemically, Cal-I calcites contain relatively high REE(Y) (151–2296 ppm), Sr (4947–9566 ppm) and Na (29–390 ppm) contents, characterized by right- to left-inclined flat distribution patterns $[(La/Yb)_N = 0.2–4.2]$ with enrichment of HREE(Y) (136–774 ppm), whereas Cal-II calcites display low REE, Sr and undetectable Na contents, characterized by a right-inclined distribution pattern $[(La/Yb)_N = 13.5, n = 16]$. The U–Nb–REE mineralization, accompanied with intense and extensive fenitization and biotitization, is mainly associated with the Cal-I-3 calcites which show flat to relatively left-inclined flat REE distribution patterns $[(La/Yb)_N = 0.2–1.0]$. Isotopic results show that Cal-I calcites with mantle signatures are primarily igneous in origin, whereas Cal-II are hydrothermal, postdating the U–Nb–REE mineralization. Cal-I calcites (Cal-I-1, Cal-I-2 and Cal-I-3) from mineralized and unmineralized carbonatites, displayed regular changes in REE, Na and Sr contents, but similar trace element distribution patterns and Sr–Nd–C–O isotopic signatures, indicating that these carbonatites originated from the same enriched mantle (EM1) source by low-degree partial melting of HREE-rich carbonated eclogites related to recycled marine sediments. The combination of trace elements and Sr–Nd isotopic composition of calcites further reveals that these carbonatites have undergone highly differentiated evolution. Such differentiation is conducive to the enrichment of ore-forming elements (U–Nb–REE) in the late magmatic–hydrothermal stages owing to extensive ore-forming fluids exsolved from carbonatitic melts. The massive precipitation of the U–Nb–REE minerals from ore-forming hydrothermal fluids may have been triggered by intense fluid–rock reactions indicated by extensive and intense fenitization and biotitization. Therefore, the Huayangchuan carbonatite-related U–Nb–REE deposit may have formed by a combination of processes involving recycled U–Nb–REE-rich marine sediments in the source, differentiation of the produced carbonatitic magmas, and subsequent exsolution of U–Nb–REE-rich fluids that precipitated ore minerals through reactions with wall rocks under the transitional tectonic regime from compression to extension at the end of Late Triassic.

* Corresponding authors at: State Key Laboratory of Ore Deposit Geochemistry, Institute of Geochemistry, Chinese Academy of Sciences, Guiyang 550081, China (R.-Z. Hu and Y.-W. Chen).

E-mail addresses: chenyouwei@mail.gyig.ac.cn (Y.-W. Chen), huruizhong@mail.gyig.ac.cn (R.-Z. Hu).

1. Introduction

Carbonatites are a rare variety of igneous rocks enriched in niobium (Nb), rare earth elements (REE), uranium (U), thorium (Th), phosphorous (P), strontium (Sr), barium (Ba), and other incompatible elements (Gittins, 1988). Some of carbonatites are characterized by Nb-REE mineralization, rendering them to be of special economic importance, and hence attracting the scientific community. Earlier studies report that carbonatites comprise approximately 51.4% of rare earth oxide (REO) resources and a majority of Nb resources on earth (Weng et al., 2015; USGS, 2020), such as, the Bayan Obo REE–Nb–(Th) deposit (China), Mountain Pass REE deposit (America), Araxá, Catalão Nb deposit, and Morro dos Seis Lagos Nb deposit (Brazil). Uranium is generally produced as a co- or by-product in rare carbonatite-related deposits, e.g., Palabora and Araxá (IAEA, 2009), Prairie Lake (Sage, 1987), Manitou Islands (Woolley, 1987), Sandkopsdrif (Verwoerd, 1986), Cummins Range (Jaques, 2008). However, such deposits with U-Nb-REE as the main resources are extremely limited. Recently, the Huayangchuan carbonatite-related deposit in the Qinling orogenic belt was recognized as a giant uranium polymetallic deposit, accompanied by remarkable Nb-REE mineralization (Nb: 0.11 Mt, 0.019%; REE: 0.55 Mt, 0.085%) (Gao et al., 2017), as a rare case of carbonatite-related U–Nb–REE mineralization.

Previous studies have shown that the carbonatites in the Huayangchuan deposit are mainly composed of calcite and aegirine–augite (Yu, 1992; Qiu et al., 1993; Xu et al., 2007). The U–Nb mineralization is mainly characterized by betafite-U–Nb [Formula: $(Ca,U)_{2-x}(Ti,Nb,Ta)_2O_6(OH,F)$], while REE mineralization is mainly characterized by monazite–Ce and allanite–Ce (Kang et al., 2018; Gao et al., 2019). However, the timing of mineralization was not tightly constrained, as available dating results show a huge range of ages from 129 to 229 Ma (Qiu et al., 1993; He et al., 2016; Gao et al., 2019; Xue et al., 2020; Zheng et al., 2020a). The genesis of the carbonatites was highly debatable, and was suggested to be related to low partial melting of garnet-poor mantle (Xu et al., 2007), liquid immiscibility of carbonate-rich alkaline magma (Qiu et al., 1993), or alkaline silicate–carbonate melt immiscibility combined with crystal fractionation (Hui et al., 2017; Xue et al., 2020). Other studies stated that subducted sediments recycled and re-melted in the mantle to generate carbonatite magmas that subsequently formed the deposit through crystal fractionation (Gao et al., 2019; Xue et al., 2020) and that the betafite mineralization resulted from the decrease in fluorine concentration due to fluorapatite crystallization (Xue et al., 2020). Moreover, some researchers suggested that the carbonatite magmas were further enriched by reactions with Proterozoic U–REE-rich pegmatitic wall rocks (Zheng et al., 2020b) or assimilation of surrounding rocks (Chen, 2019). In summary, the genesis of Huayangchuan carbonatites and related U–Nb–REE mineralization is still controversial. One of the reasons for these controversies is the lack of detailed mineralogical studies based on various carbonatitic facies. Calcite is the dominant mineral in Huayangchuan carbonatites and it occurs in all carbonatitic facies. Importantly, some stage of calcite is associated with the main ore minerals such as betafite-U–Nb and monazite–Ce. Additionally, it has high trace elements (e.g., Sr, Mn and Na) and REE (including Sm and Nd) contents. These trace elements and some isotopes (C–O–Sr–Nd) can effectively trace the genetic evolution of carbonatites and associated critical metal mineralization (Ionov and Harmer, 2002; Yang and Le Bas, 2004; Xu et al., 2007; Chen and Simonetti, 2013; Chakhmouradian et al., 2016).

In this study, we conducted detailed textural, chemical and Sr–Nd–C–O isotopic investigations on multi-type calcites in this deposit. The new dataset allows us to (1) constrain the petrogenesis of carbonatites, (2) reveal origin of the unique U–Nb–REE polymetallic mineralization, and (3) ultimately build the metallogenetic model of the Huayangchuan deposit. Our study will provide new insights on the origin of similar carbonatite-related deposits worldwide.

2. Geology of the Huayangchuan deposit

The Qinling orogenic belt (QLOB), an important tectonic unit in central China (Fig. 1a), underwent a prolonged and complex tectonic evolution (Meng and Zhang, 1999). The first collision of the South Qinling (SQL) and North Qinling (NQL) took place in Middle Paleozoic along the Shang-Dan suture (SDS) and were subsequently separated during the middle to late Paleozoic (Meng and Zhang, 1999, 2000). The QLOB was eventually formed by the collision between South China Craton (SCC) and North China Craton (NCC) along the Mian-Lüe suture (MLS) zone owing to closure of Qinling Ocean during Late Triassic (Meng and Zhang, 1999, 2000). The NQL and SQL are separated by SDS and the QLOB can be divided into four parts based on the main deep fractures of MLS, SDS, Luan-Chuan fault (LCF) and San-Bao fault (SBF), that is, south margin of the North China Craton (S-NCC), the NQL belt, the SQL belt and north margin of the South China Craton (N-SCC) (Fig. 1b) (Zhang et al., 2004). In addition, there is one of the most important alkaline igneous provinces of China distributing along the Qinling belt, which strikes near E–W from west Qinling to east Qinling and Dabie and can be subdivided into northern and southern sections (Qiu et al., 1993). Regional geological studies have confirmed that numerous carbonatite complexes are emplaced on the northern and southern sides of east Qinling (Li, 1982; Yu, 1992; Qiu et al., 1993; Xu et al., 2014). The southern section of the eastern Qinling is predominantly represented by the Miaoya and Shaxiongdong alkaline carbonatite complexes (Li, 1982; Qiu et al., 1993; Xu et al., 2008), while the northern section of the eastern Qinling Mountains is mainly represented by the Huayangchuan, Dashigou and Huangshui'an carbonatite complexes, extending nearly 200 km in E–W direction.

The Huayangchuan carbonatites, located in northern section of the Qinling alkaline igneous belt (Fig. 1b), intruded the meta-sedimentary rocks of the Archean Taihua Group (Huang et al., 1985; Yu, 1992; Qiu et al., 1993) and cut the Paleoproterozoic granite porphyry and granite pegmatite (Xue et al., 2020). The northern and southern parts of the carbonatite distribution area are the Huashan and Laoniushan granitoid plutons (Fig. 1c). Carbonatite dykes striking W–NW (290–310°) direction, controlled strictly by the Huayangchuan fault, are 500–1000 m wide, and approximately 6000 m in length (Fig. 1c). These carbonatites are the major host of U–Nb–REE orebodies which are characterized by stockworks (Fig. 2a). Single carbonatite dyke is generally short in length, and several centimeters to meters in width. The ore district has been extensively altered due to fenitization, biotitization, and silicification. Based on the field geological works and the petrographic characteristics, quartz calcite carbonatite, aegirine-augite calcite carbonatite, biotite calcite carbonatite and zeolite-calcite veins have been identified (Fig. 2b–f). Cross-cutting relationships reveal that the early quartz calcite carbonatite (Fig. 2b) has been intruded by aegirine-augite calcite carbonatite and biotite calcite carbonatite (Kang et al., 2018) and, subsequently by the latest zeolite-calcite veins (Fig. 2f). The U–Nb–REE mineralization mainly occurs in the contact zones between carbonatites and wall rocks accompanying widespread intense fenitization and biotitization (Fig. 2e and f), where the wall rocks are generally loose and broken in the absence of strong silicification. In contrast, at sites where early fresh quartz calcite carbonatites have clear boundaries with strongly silicified wall rocks (Fig. 2b), the carbonatites possess low metallogenetic potential due to the presence of negligible fenitization and biotitization. Furthermore, carbonatites associated with complex mineral assemblage (Fig. 2c and d) are usually accompanied by significant U–Nb–REE mineralization. Such carbonatites with complex mineral assemblages or such zones with intense and extensive fenitization and biotitization in contact with carbonatite and wall rock are the dominant ore producing locations in the ore district (Fig. 2c and d). Mineralized calcite carbonatites (MCC) have been severely weathered, resulting in large amounts of black Mn oxides and quartz relicts (Fig. 2d).

According to the mineral assemblages, the U–Nb–REE-bearing ore

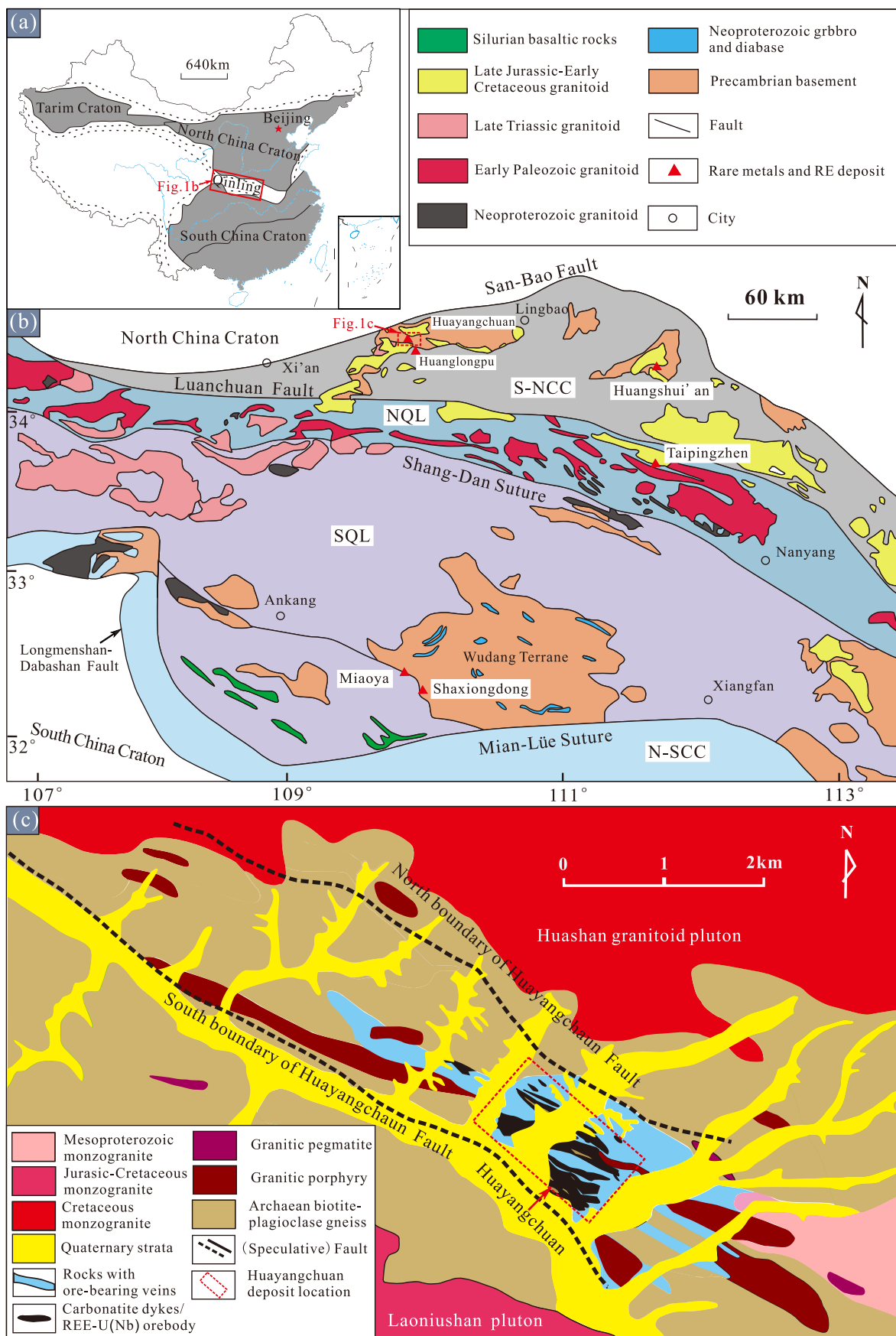


Fig. 1. Geological map of the study area. (a) Tectonic map of China. (b) Simplified geological map of the Qinling orogenic belt (modified after Zhang et al., 2019). (c) Regional geological sketch map of the Huayangchuan district (modified after Gao et al., 2017).

types can be divided into: (1) fine-grained aegirine–augite calcite carbonatites (Fig. 2c and d), (2) pink–white biotite calcite carbonatite orebodies associated with biotitization and fenitization (Fig. 2e), and (3) minor hydrothermal vein-type ore. The aegirine–augite calcite carbonatite-type ores are composed of calcite, aegirine-augite, bafatite-(U-Nb), apatite, quartz, galena, pyrite and barytocelestite (Fig. 3a–d). The dominant mineral assemblages for biotite calcite carbonatite-type ore are calcite, biotite, K-feldspar, barytocelestite, bafatite-(U-Nb), monazite-(Ce), allanite-(Ce) and apatite with minor molybdenite, samarskite-(Y-Nb), uraninite and titanite (Fig. 3e–h), and those for hydrothermal ore-type are bafatite-(U-Nb), monazite-(Ce), allanite-(Ce), apatite, and barytocelestite (Fig. 3i). Detailed fresh petrographic features have been shown in Fig. 4. Three stages and their paragenetic sequence for deposit are summarized in Fig. 5.

3. Mineralogical evolution and paragenesis

Based on crosscutting relationship, mineral assemblages and textures of calcite-related veins, calcites can be divided into two principal types (Cal-I and Cal-II), the Cal-I can be subdivided into three sub-types: Cal-I-1, Cal-I-2, Cal-I-3.

3.1. Cal-I calcites

Cal-I calcites occur in association with aegirine–augite, along with minor quartz, amphibole and barytocelestite as calcite cumulates with grain size varying in the range 200 µm–0.5 cm (Fig. 4). Cal-I calcites can be further categorized into three sub-types as follows:

(1) Cal-I-1 calcites

The coarse-grained Cal-I-1 calcites occur in premineralization stage (early magmatic stage) and exhibit an equigranular cumulate texture (~0.5 cm) with a clean surface, and paragenesis with pegmatitic quartz (Fig. 2b and 4a). The coarse-grained quartz calcite carbonatites show a clear boundary with silicified wall rocks (Fig. 2b) and have hardly been mineralized with negligible fenitization and biotitization.

(2) Cal-I-2 calcites

The Cal-I-2 calcites are a transitional sub-type in aegirine-augite calcite carbonatite and biotite calcite carbonatite, composing chiefly of euhedral to subhedral medium-grained calcites (500–2000 µm) and few fine-grained calcites (~500 µm), exhibiting an intergranular texture (Fig. 3d, 4g and 12b). This sub-type is usually accompanied by a large amount of aegirine-augite, minor amphibole, phlogopite (Fig. 4b and c). Cross-cutting relationship reveals that the Cal-I-2 calcite crystals were cut by fine-grained Cal-I-3 calcite veinlets (Fig. 3d).

(3) Cal-I-3 calcites

The anhedral fine-grained Cal-I-3 calcites occur in U-Nb-REE mineralization stage (late magmatic to hydrothermal stage) and exhibit an equigranular texture (200–500 µm) in aegirine-augite calcite carbonatite and biotite calcite carbonatite. The mineral assemblage in fresh un-mineralized calcite carbonatite (UMCC) is extremely simple, nearly homogeneous calcite with minor barytocelestite and apatite (Fig. 4d, h), showing a fuzzy dirty surface, indicating small amounts of carbonatite-exsolved fluids (Fig. 4h). Interestingly, the U-Nb-REE minerals (e.g., bafatite, monazite, allanite, samarskite) in MCC primarily coexist with late fine-grained Cal-I-3 calcites (Fig. 3b-e and g) accompanied by fenitization and biotitization (Fig. 2e). Other minerals paragenetic with this stage calcite are biotite, aegirine-augite, K-feldspar, titanite, galena, pyrite, minor molybdenite and uraninite (Fig. 5). Barytocelestite precipitated slightly later than sulfides (Fig. 5). Additionally, cathodoluminescence (CL) images reveal that Cal-I-3 calcites in the mineralized samples suffered intense fluid metasomatism displaying a core–rim texture (Fig. 3c).

3.2. Cal-II calcites

Cal-II calcites occur in association with zeolite and minor galena, pyrite, apatite, and quartz in the form of post-mineralized zeolite–calcite veins (PMZV) infilling gneissic fissures (Fig. 2f and 4e, j). Mineral assemblages reveal that zeolite–calcite veins formed in the late low-temperature hydrothermal conditions.

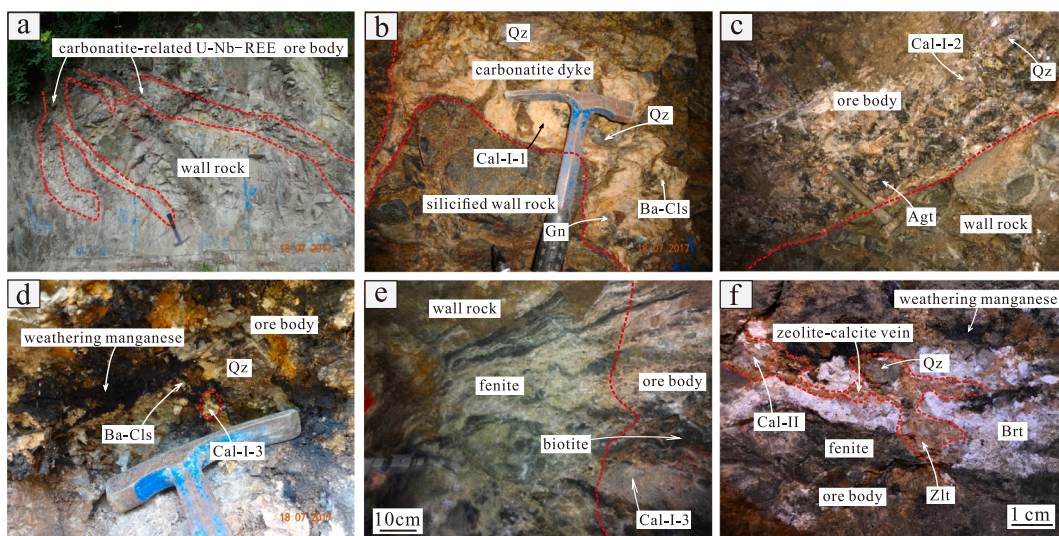


Fig. 2. (a) U-Nb-REE ore bodies associated with carbonatite dykes intruding the biotite-plagioclase gneiss of the Taihua Group in reticulated veins. (b) Quartz calcite carbonatite dykes accompanying the silicified wall rocks. (c) U-Nb-REE-bearing aegirine-augite calcite carbonatite dykes. (d) Barytocelestite, quartz and calcite developed in ore bodies, associated with weathered supergene manganese. (e) Ore body for biotite calcite carbonatite dykes associated with intensive fenitization and biotitization. (f) Ore body associating with fenites cut by the late zeolite–calcite veins. Abbreviations: Qz, quartz; Ba-Cl, barytocelestite; Gn, galena; Agt, aegirine-augite; Brt, barite; and Zlt, zeolite.

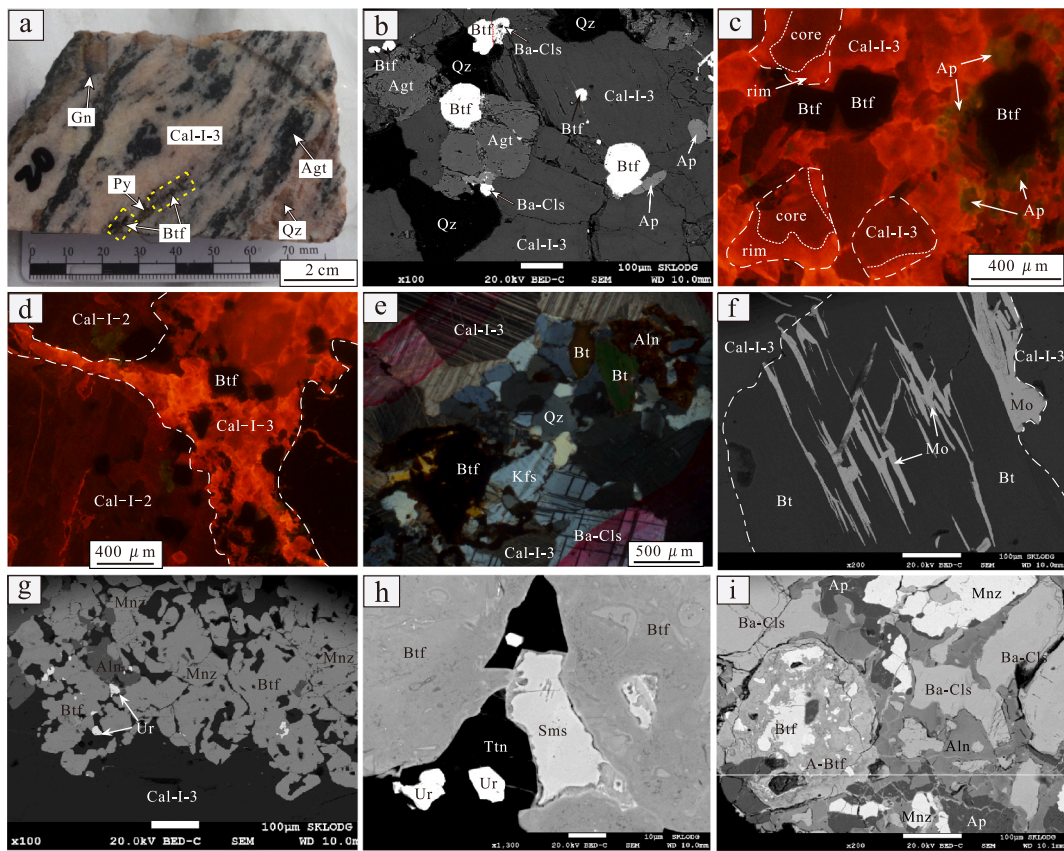


Fig. 3. Petrographic images illustrating the features of mineral assemblages in typical mineralized samples at Huayangchuan U–Nb–REE polymetallic deposits: (a,b) Mineralized fine-grained aegirine–augite calcite carbonatites with mineral assemblages of betafite–(U–Nb), apatite, barytocelestite, calcite, aegirine–augite, pyrite, galena, and quartz. (c) CL image displaying betafite precipitated with apatite, along with fine-grained calcite with a typical core–rim texture. (d) Cross-cutting relationships reveals that the medium-grained calcite crystals were cut across by fine-grained calcite veinlets. BSE image showing the betafite paragenesis with samarskite–(Y–Nb) and titanite. (e–h) Mineralized fine-grained biotite calcite carbonatites in the late stage associated with U–Nb–REE mineralization with mineral assemblage of betafite–(U–Nb), monazite–(Ce), allanite–Ce, biotite, molybdenite, calcite, K-feldspar, barytocelestite, quartz and uraninite. (i) Hydrothermal vein type ore body showing mineral assemblages of betafite, monazite, apatite, allanite and barytocelestite. Abbreviations: Btf, betafite; Mnz, monazite; Aln, allanite; Ap, apatite; Sms, samarskite; Ur, uraninite; Ttn, titanite; Cal, calcite; Bt, biotite; Kfs, K-feldspar; Agt, aegirine-augite; Qz, quartz; Ba-Cl_s, barytocelestite; Gn, galena; Mo, molybdenite; and Py, pyrite.

4. Analytical methods

Samples were collected from the field and the drill hole at the Huayangchuan U–Nb–REE deposit. The calcites in the samples were analyzed for mineralogy, in situ calcite major and trace element compositions, in situ calcite Sr–Nd isotopes, and bulk C–O isotopic characteristics. The analyses were carried out at the State Key Laboratory of Ore Deposit Geochemistry, Institute of Geochemistry, Chinese Academy of Sciences, Guiyang, China.

4.1. Mineralogical analyses

Mineralogy and crosscutting textures were investigated on the polished thin sections using a conventional optical microscope. A JEOL JSM–7800F field emission scanning electron microscope (FE-SEM) equipped with EDAX TEAM Apollo XL energy-dispersive spectroscopy (EDS) was used as an effective tool to identify fine-grained minerals and to obtain backscattered electron (BSE) images.

4.2. In situ major and trace element analyses

Major element compositions of calcites were measured using a JEOL–JAX8230 electron microprobe (EMP) with a 15 kV accelerating potential, 12nA beam current, 5 μm beam spot, and 10–30 s counting

time on different peaks.

Trace element composition analyses (including REE) of calcites were conducted using laser ablation ICP–MS and a Coherent GeoLas MV 193 nm laser ablation system combined with an Agilent 7700x ICP–MS. Spot analyses of calcites were bracketed with replicate analyses of reference material NIST SRM 610 to correct for instrumental drift and as an external standard. The Ca content of calcites analyzed by EMP was used as an internal standard calibration.

4.3. In situ Sr–Nd isotopic analyses

In situ calcite Sr–Nd isotopic measurements were conducted on a Nu Plasma III MC–ICP–MS (Nu Instruments) attached to a RESolution-155 ArF193-nm laser ablation system (Australian Scientific Instruments).

When testing the Sr isotopes of calcite, samples were ablated in a mixture of helium (350 mL/min) and nitrogen (2 mL/min) gases using the following parameters: 30 s baseline time, 40 s ablation time, 32–104 μm spot size, 6 Hz repetition rate, and 6 J/cm² energy density. The analytical and interference correction protocols followed the method described by Ramos et al. (2004). Two standards, a modern-day coral after every five samples and apatite (AP2) after every ten unknown samples, were used for quality control. The measured ⁸⁷Sr/⁸⁶Sr ratio for modern-day coral calcite standard is 0.709184 ± 37 (n = 27), which is identical to the Sr isotopic ratio of the modern sea, 0.709172 (Hodell

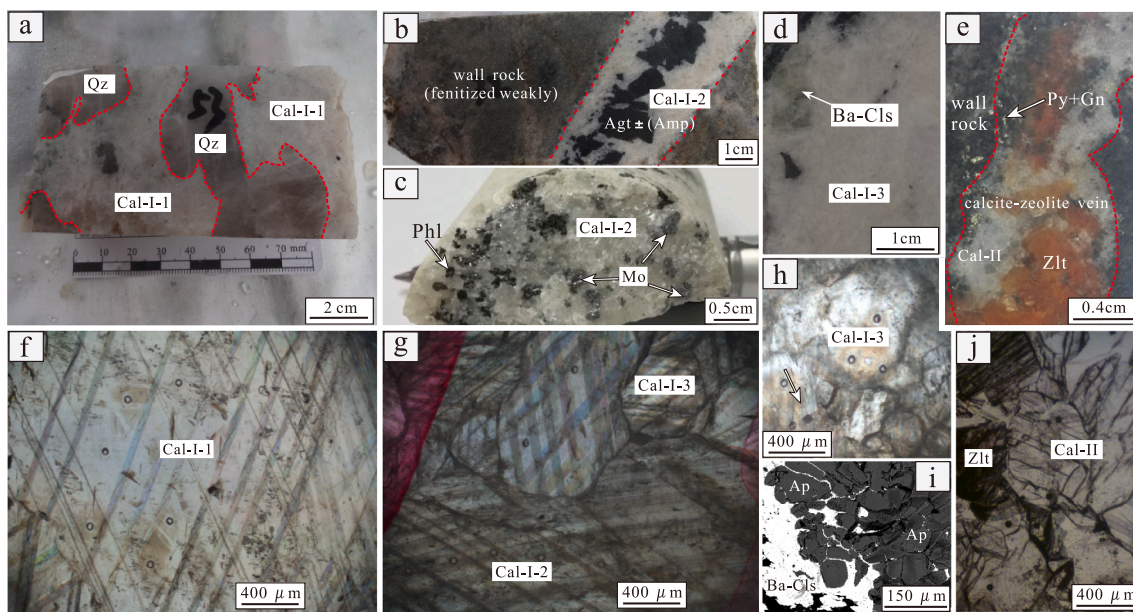


Fig. 4. Images illustrating the occurrence and key petrographic features of virous unmineralized calcite carbonatites and carbonate veins at Huayangchuan. (a) Hand specimen and optical photograph showing coarse-grained calcite (Cal-I-1: ~0.5 cm) occurring with the quartz calcite carbonatite cumulates (see barytocelestite) in the early stage. (b) Hand specimen and optical photograph showing medium-grained calcite crystals (Cal-I-2: 500–2000 μm) occurring with aegirine–augite calcite carbonatites. (c) Calcite carbonatite cumulates (see phlogopite and molybdenite) in the middle stage. (d, h-i) Hand specimen and optical and BSE images showing fine-grained calcite (Cal-I-3: 200–500 μm) occurring with the calcite carbonatite cumulates (mineral assemblages of calcite, apatite and barytocelestite) in the late stage. (e, j) Hand specimen and optical photograph showing the hydrothermal calcite (Cal-II) occurring with calcite–zeolite veinlets with paragenesis of pyrite, galena, apatite, and quartz. Abbreviations: Cal, calcite; Agt, aegirine-augite; Phl, Phlogopite; Qz, quartz; Ba-Cl's, barytocelestite; Gn, galena; Mo, molybdenite; Py, pyrite; and Amp, amphibole.

et al., 1990). The measured $^{87}\text{Sr}/^{86}\text{Sr}$ ratio for apatite standard AP2 was 0.72653 ± 0.00005 ($n = 10$), which is identical to the recommended value of 0.72655 ± 0.00002 (Yang et al., 2009).

For the Nd isotopic analysis of calcites, 154–228 μm spot size, 6 Hz repetition rate, and 6 J/cm² energy density were used. The interference of ^{144}Sm on ^{144}Nd was derived from the ^{147}Sm intensity with a natural $^{144}\text{Sm}/^{147}\text{Sm}$ ratio of 0.205484 (Isnard et al., 2005). The mass bias factor of Sm was calculated from the measured $^{147}\text{Sm}/^{149}\text{Sm}$ isotopic ratio and its true value, 1.08680 (Isnard et al., 2005). The mass bias of $^{143}\text{Nd}/^{144}\text{Nd}$ was normalized to $^{146}\text{Nd}/^{144}\text{Nd} = 0.7129$ using an exponential law. An apatite standard (AP1) was used as quality control after every five samples. The measured $^{143}\text{Nd}/^{144}\text{Nd}$ ratio for AP1 was 0.512342 ± 0.000014 ($n = 12$), which is identical to the recommended value (AP1: 0.512352 ± 0.000024) (Yang et al., 2014).

4.4. Bulk C–O isotopic analyses

Calcite grains were separated from carbonatites and zeolite–calcite carbonate veins for C and O isotopic analyses. Calcite powder was collected on a weighing paper and transferred to a standard 12 mL headspace sample vial or a 3 mL small vial, depending on the sample size. Then, the samples were flushed with helium using a Gasbench II device (Thermo Fisher Scientific, Breman, Germany) for 8 min. Phosphoric acid was manually dosed to the flushed samples to analyze CO₂. The sample and acid were reacted at 72 °C for at least 4 h and were then measured for $\delta^{13}\text{C}$ and $\delta^{18}\text{O}$ using a Gasbench II device attached to a MAT 253 gas source isotope ratio mass spectrometer (Thermo Fisher Scientific).

5. Results

5.1. In situ major and trace element compositions

The in situ major and trace element contents of the two calcite types

are listed in Tables A1 and A2. The mean values of trace-element composition of calcites from carbonatites and zeolite–calcite veins are presented in Table 1.

The major element composition of Cal-I calcites are as follows: CaO (52.34–54.50 wt%), MgO (0.09–0.64 wt%), SrO (0.79–1.20 wt%), FeO (0.57–0.86 wt%) and MnO (0.71–1.84 wt%); those for Cal-II calcites are: CaO (53.58–55.90 wt%), MgO (<0.10 wt%), SrO (<0.28 wt%), FeO (<0.28 wt%) and MnO (0.57–2.35 wt%). Cal-II calcites have lower MgO, SrO (<0.28 wt%), FeO, relatively higher CaO, and widely variable MnO (0.57–2.35 wt%) contents compared to Cal-I. All calcites have a high MnO content.

Compared to the trace element analysis results for Cal-II, Cal-I calcites (Cal-I-1, Cal-I-2, and Cal-I-3) show high $\sum\text{REE}$ (62–1984 ppm, av. 654 ppm), $\sum\text{REY}$ (lanthanides and Y, 151–2296 ppm, av. 921 ppm), $\sum\text{HREY}$ (Gd–Lu and Y, 136–774 ppm, av. 426 ppm), Y (89–474 ppm, av. 267 ppm), Na (29–390 ppm, av. 162 ppm), Mg (621–3652 ppm, av. 1734 ppm), Mn (5348–12287 ppm, av. 9124 ppm), Fe (2924–6077 ppm, av. 4174 ppm), Sr (4947–9566 ppm, av. 7607 ppm), Pb (20–171 ppm, av. 91 ppm), Ba (4–35 ppm, av. 10 ppm), P (<127 ppm, av. 57 ppm), Zn (2–24 ppm, av. 7 ppm), and In (<1.11 ppm, av. 0.53 ppm) contents. All the calcite samples have low Rb, Co, As, Th, U, Nb, Zr, and Hf contents, and some elemental contents are even lower than the detection limit.

The trace element spider diagram (Fig. 6) shows that the Cal-I calcites display characteristics similar to those rich in Pb, Sr, and REE, and are significantly depleted in Rb, Th, U, Nb, P, Zr, and Hf. However, calcites in the mineralized stages (Cal-I-3) were relatively enriched in U and Nb compared to Cal-I-1 calcites. Cal-II calcites have lower REE, Ba, Pb, and Sr contents than Cal-I calcites. Significant differences in the REE distribution patterns of Cal-I and Cal-II calcites can be seen from Fig. 7. Cal-I calcites are generally characterized by right- to left-inclined flat distribution patterns $[(\text{La/Yb})_N = 0.2–4.2]$ with HREE enrichment, while Cal-II calcites are characterized by a right-inclined distribution pattern $[(\text{La/Yb})_N = 13.5, n = 16]$ with LREE enrichment and significant depletion of HREE. Similar to reports by Xu et al. (2007), Cal-I calcites

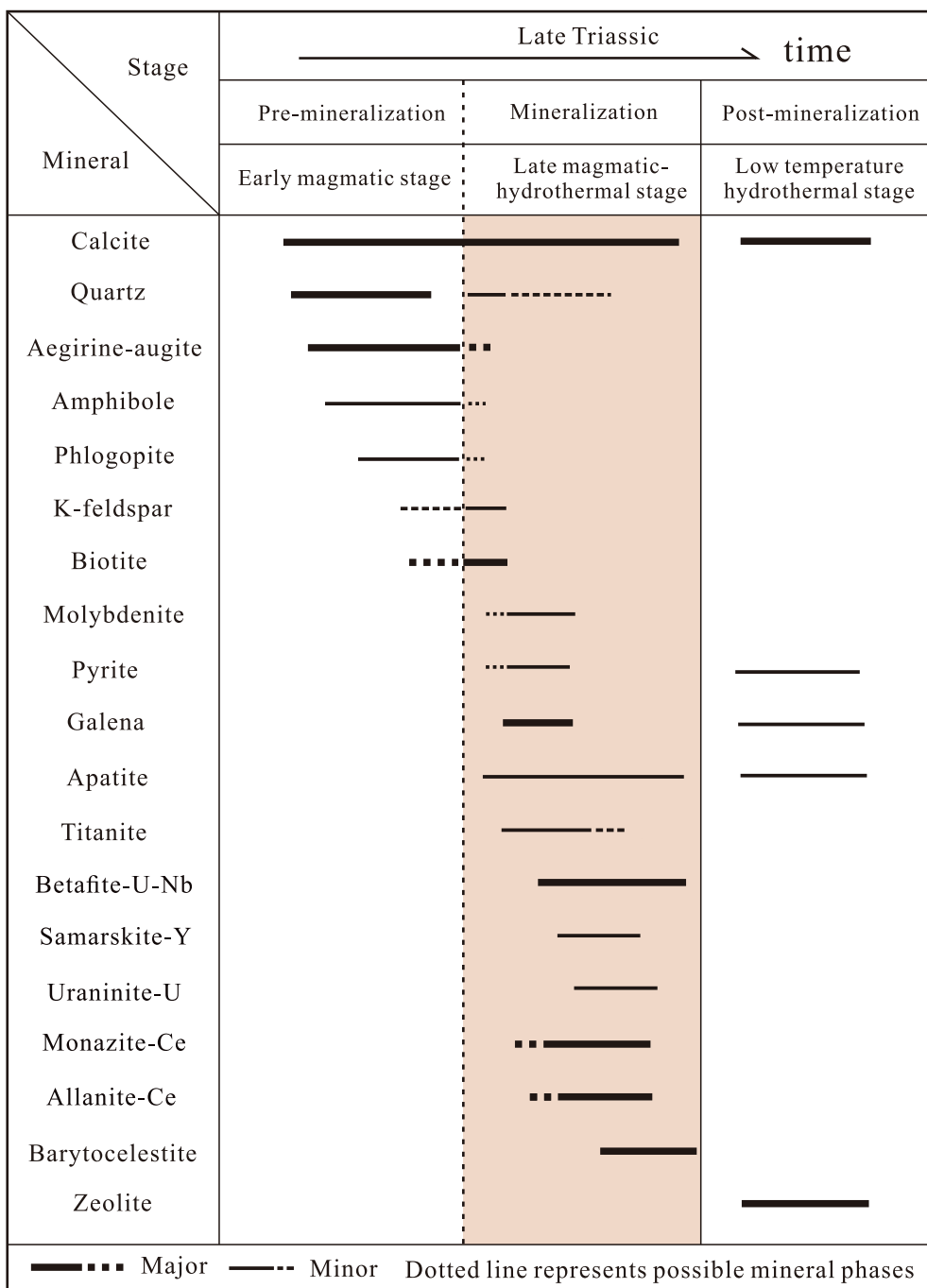


Fig. 5. Summary of the mineral paragenesis at the Huayangchuan deposit.

(Cal-I-1, Cal-I-2, and Cal-I-3) from fresh unmineralized carbonatitic samples are characterized by right-inclined flat distribution patterns $[(\text{La/Yb})_N = 0.9\text{--}4.2]$ with slight LREE enrichment. However, in this study, we noted that calcites (Cal-I-2 and Cal-I-3) in mineralized samples displayed flat to relatively left-inclined flat distribution patterns $[(\text{La/Yb})_N = 0.2\text{--}1.0]$. We further reported that LREE decreases steadily while HREE increases slightly from Cal-I-1 to Cal-I-2 and Cal-I-3 in unmineralized calcite carbonatites, showing a gradation.

5.2. In situ calcite Sr-Nd isotopes

The results of in situ calcite Sr-Nd isotopes are presented in Table A3. Our previous geochronological work based on uraninite grains coexist with betaafite revealed that the Huayangchuan carbonatite-related U-Nb-

REE deposit was formed at ca. 201 Ma at the end of Late Triassic (Gao et al., 2019), which is also supported by the dating work of titanite (209 Ma) and molybdenite (197 Ma) (Zheng et al., 2020a), therefore, initial Sr-Nd isotopic values were calculated based on 200 Ma. The $(^{87}\text{Sr}/^{86}\text{Sr})_i$ and $(^{143}\text{Nd}/^{144}\text{Nd})_i$ isotopic values for all calcites range from 0.704851 to 0.706646 and 0.511549 to 0.512204, respectively.

Initial Sr and Nd isotopic values for Cal-I calcites from fresh unmineralized carbonatitic samples show a tight cluster ranging from 0.704851 to 0.704999 (av. 0.704940, $n = 29$) and 0.511984 to 0.512114 (av. 0.512058, $n = 29$), respectively, similar to the results reported by Xu et al. (2011). Sr and Nd isotopic compositions in Cal-I calcites of aegirine-augite calcite carbonatites ranged from 0.704896 to 0.705076 (av. 0.704977, $n = 41$) and 0.511843 to 0.512172 (av. 0.512003, $n = 41$), respectively, while those for biotite calcite

Table 1

Trace element compositions (ppm) of Cal-I-1, Cal-I-2, Cal-I-3 and Cal-II calcites from the Huayangchuan carbonatites and post-mineralized zeolite-calcite veins (mean values).

Rock type	White calcite carbonatite			Aegirine-augite calcite carbonatite		Biotite calcite carbonatite		Zeolite calcite vein	
	Calcite from unmineralized carbonatites (Cal-I)			Calcite from mineralized carbonatites (Cal-I)			Calcite from post-mineralized zeolite calcite veins (Cal-II)		
	Cal-I-1 (n=14)	Cal-I-2 (n=9)	Cal-I-3 (n=27)	Cal-I-2 (n=23)	Cal-I-3 (n=27)	Cal-I-2 (n=6)	Cal-I-3 (n=19)	Cal-II (n=16)	
Rb	0.02	0.04	0.05	0.01	0.01	0.02	0.04	0.01	
Ba	10.6	7.2	8.3	8.6	9.5	10.0	17.1	0.1	
Th	0.004	0.15	0.007	0.003	0.07	0.002	0.009	0.03	
U	0.001	0.01	0.01	0.050	0.09	0.003	0.06	0.01	
Nb	0.001	0.001	0.008	0.180	0.10	0.003	0.04	0.000	
La	164	106	50	32	7	35	37	34	
Ce	535	406	235	121	32	99	103	31	
Pb	104	128	95	123	36	128	85	0.4	
Pr	76.5	66.0	42.0	20.5	6.2	14.8	15.2	3.1	
Sr	8635	8218	8719	7429	6489	7387	6856	588	
P	55	82	51	52	22	51	48	5	
Nd	365	336	245	116	39.9	79	78	14	
Sm	81.4	84.3	79.1	33.4	14.6	25.3	21.8	2.7	
Zr	0.03	0.02	0.03	0.02	0.03	0.00	0.02	0.03	
Hf	0.02	0.02	0.03	0.01	0.01	0.02	0.00	0.02	
Eu	21.2	23.5	24.3	10.2	5.0	8.5	6.6	1.3	
Gd	65.2	71.8	79.0	35.3	19.4	33.0	24.4	3.5	
Tb	8.54	9.42	11.16	5.04	3.00	5.66	3.79	0.41	
Dy	46.1	52.7	62.9	30.7	19.8	38.2	24.1	2.4	
Y	283	321	415	226	169	288	200	26	
Ho	9.27	10.50	12.89	6.94	4.84	8.78	5.66	0.57	
Er	25.9	29.6	36.7	21.6	15.9	27.5	18.6	1.6	
Tm	3.83	4.45	5.57	3.45	2.70	4.44	3.11	0.22	
Yb	26.5	31.5	39.7	25.4	21.2	33.7	25.0	1.7	
Lu	3.77	4.39	5.63	3.84	3.38	5.08	4.09	0.32	
Co	0.28	0.28	0.28	0.16	0.14	0.10	0.10	0.06	
Zn	7.85	8.78	9.42	6.70	3.86	4.99	8.43	0.00	
As	2.22	2.30	1.50	0.67	0.10	0.30	0.36	0.10	
In	0.49	0.57	0.50	0.51	0.45	0.79	0.58	0.04	
Cd	0.36	0.76	0.49	0.65	0.54	1.11	0.77	0.06	
Ni	0.46	0.23	0.22	0.28	0.29	0.05	0.07	0.12	
(La/Yb) _N	4.22	2.30	0.86	0.87	0.24	0.70	1.00	13.54	

Note: Mean values of U, Th, Nb, Zr, Hf contents in most of the measuring samples are below detection limit, and the mean values of these elements are given for plotting purposes only, with the exception of calcite from a few mineralized carbonatic samples with relatively high U and Nb contents. n, Number of LA-ICPMS spot analyses.

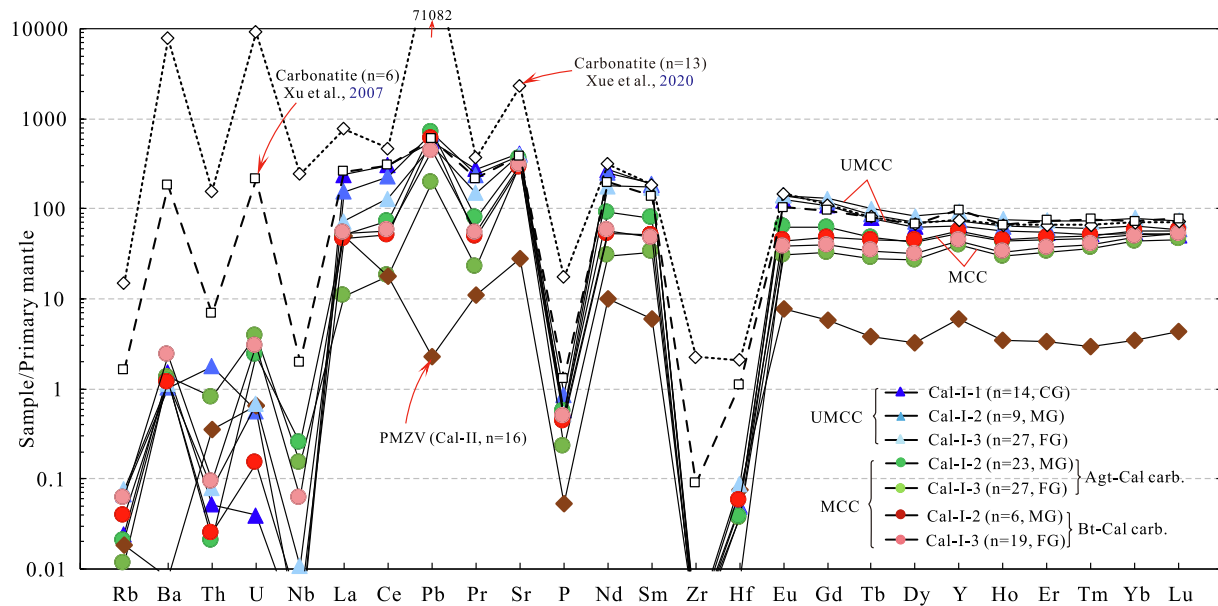


Fig. 6. Trace elemental abundances (mean values) for different calcite types at Cal-I-1, Cal-I-2, Cal-I-3, and Cal-II stages. Normalization values for trace element abundances obtained from Sun and McDonough (1989). Abbreviations: Agt, aegirine-augite; Bt, biotite; Cal, calcite; Zlt, zeolite; Carb., carbonatite; UMCC, calcites from the un-mineralized calcite carbonatite; MCC, calcites from the mineralized calcite carbonatite; PMZV, calcites from the post-mineralized zeolite-calcite veins; CG, coarse-grained; MG, medium-grained; FG, fine-grained.

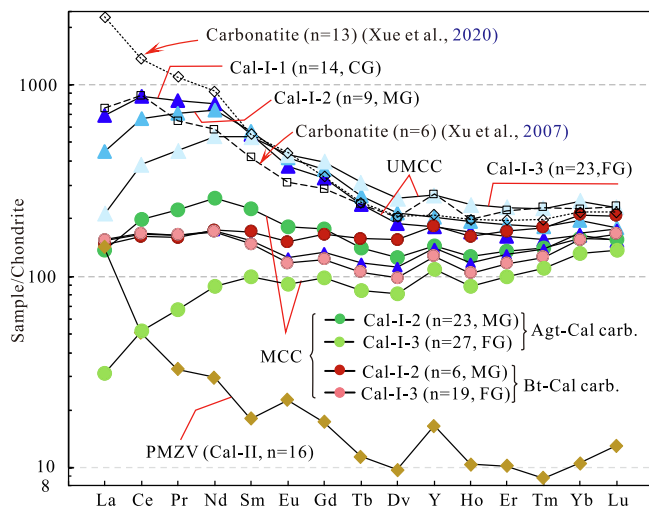


Fig. 7. REE distribution patterns for different calcite types (mean values) at different stages. Normalization values for REE distribution patterns are from McDonough and Sun (1995).

carbonatites ranged from 0.705413 to 0.706086 (av. 0.705657, $n = 19$, relatively high Sr isotopic values) and 0.511945 to 0.512204 (av. 0.512065, $n = 19$), respectively. However, compared to calcites in carbonatites, Cal-II calcites from the zeolite–calcite veins have relatively higher Sr isotope ratios ranging from 0.706252 to 0.706646 (av. 0.706441, $n = 17$) and lower Nd isotope ratios ranging from 0.511549 to 0.512010 (av. 0.511791, $n = 17$). Note that we cannot exactly evaluate the isotopic results for specific mantle endmembers because most of the ocean floor is <180 Ma (Tarbuck and Lutgens, 2017).

5.3. Calcite C–O isotopes

The results of bulk carbon and oxygen isotopes from different types of calcites are presented in Table 2. The carbon isotope values for all calcites range from $-11.01\text{\textperthousand}$ to $-6.76\text{\textperthousand}$, and oxygen isotope values range from $6.86\text{\textperthousand}$ to $15.30\text{\textperthousand}$. Cal-I calcites from unmineralized carbonatites have narrow $\delta^{13}\text{C}_{\text{VPDB}}$ values ranging from $-7.09\text{\textperthousand}$ to $-6.77\text{\textperthousand}$, and $\delta^{18}\text{O}_{\text{VSMOW}}$ values ranging from $6.86\text{\textperthousand}$ to $8.78\text{\textperthousand}$; Cal-I calcites from mineralized carbonatites have narrow $\delta^{13}\text{C}_{\text{VPDB}}$ values ranging from $-7.49\text{\textperthousand}$ to $-6.76\text{\textperthousand}$, and $\delta^{18}\text{O}_{\text{VSMOW}}$ values ranging from $8.09\text{\textperthousand}$ to $9.70\text{\textperthousand}$. The entire carbon and oxygen isotopic data for Cal-I calcites plot in the primary igneous carbonatite (PIC) field and represent mantle-derived compositions. However, $\delta^{13}\text{C}_{\text{VPDB}}$ ($-11.01\text{\textperthousand}$ to $-9.87\text{\textperthousand}$) and $\delta^{18}\text{O}_{\text{VSMOW}}$ ($10.86\text{\textperthousand}$ to $15.30\text{\textperthousand}$) data of Cal-II calcites from zeolite–calcite carbonate veins plot out of the PIC field, suggesting that Cal-II calcites may have had different origins or underwent other geological processes.

6. Discussion

6.1. Petrogenesis of the carbonatites

The origin of carbonatites currently remains controversial. Previous studies have proposed three main genetic models (or any combination of three models), which are: (1) direct extensive fractional crystallization from mantle-derived CO_2 -rich alkaline silicate magmas (Veksler et al., 1998a, 1998b; Verhulst et al., 2000), (2) originating from mantle-derived CO_2 -rich alkaline silicate immiscible liquid magmas (Hamilton et al., 1979; Kjarsgaard et al., 1995; Lee and Wyllie, 1996; Brooker, 1998; Xu et al., 2003; Hou et al., 2006), and (3) originating from the upper mantle by very low partial melting of carbonated peridotites or eclogites (Nelson et al., 1988; Dalton and Presnall, 1998; Dasgupta et al., 2007; Xu et al., 2007; Cheng et al., 2017). These possible genetic

mechanisms for the Huayangchuan carbonatites have been discussed in detail below.

The crystal fractionation model is characterized by the occurrence of alkaline silicate cumulate rocks such as olivinites, clinopyroxenites, and melilitolites (Verhulst et al., 2000; Bell and Rukhlov, 2004). However, field observations reveal that the igneous rocks exposed in the area are dominantly intermediate-acidic rocks (e.g., granite and granite pegmatites), with absence of contemporaneous alkaline silicate rocks (Fig. 1c and 2a–c). Furthermore, Bell and Rukhlov (2004) showed that the process of crystal fractionation leads to a carbonatitic compositional trend transitioning from early calcitic to late dolomite–ankeritic or sideritic. However, the main carbonate mineral recognized in the Huayangchuan carbonatites is calcite, with negligible amounts of dolomite or ankerite and siderite. Therefore, the crystal fractionation model for the mantle-derived CO_2 -rich silicate magma could be ruled out as the controlling mechanism for the generation of the Huayangchuan calcite carbonatites.

For carbonatite alkaline silicate complexes to be formed via liquid immiscibility, the initial isotopic signature in carbonatites should be consistent with that of conjugate alkaline silicates (Harmer and Gittins, 1998; Xu et al., 2003; Bell and Rukhlov, 2004; Hou et al., 2006). As mentioned earlier, no conjugate alkaline silicate rocks have been found at Huayangchuan. Moreover, the formation of globules is regarded as a key petrological texture feature of magma immiscibility (Ferguson and Currie, 1971; Hamilton et al., 1979; Le Bas, 1987; Kamenetsky and Yaxley, 2015), which were neither observed during the microscopic mineralogical study (Figs. 3 and 4). As such, the liquid immiscibility model for mantle-derived CO_2 -rich alkaline silicate magmas can be discounted.

The bulk C–O isotopic data of carbonatites and in situ Sr–Nd isotopic data for unmineralized igneous calcites from Cal-I-1, Cal-I-2, and Cal-I-3 (Fig. 8) support that the Huayangchuan carbonatites originated from the EM1 mantle, and are characterized by typical primary igneous carbonatite instead of a hydrothermal origin. Bell and Rukhlov (2004) summarized the genetic models of carbonatites and concluded that those formed directly by low-degree partial melting are characterized by a high Si component. Mineralogical evidence shows that the Huayangchuan carbonatites contain abundant silicate minerals (e.g., aegirine–augite, mica) (Fig. 2c and 4b–c), indicating that the Huayangchuan carbonatites are silicon-rich. Experimental studies have shown that low-degree partial melting of carbonated peridotites generates magnesiocarbonatites (Harmer and Gittins, 1998; Ghosh et al., 2009) but unlikely generates calciocarbonatites (Ghosh et al., 2009), while low-degree partial melting of recycled carbonated oceanic crust (carbonated eclogites) generally generates calciocarbonatites (Hoernle et al., 2002). The Huayangchuan carbonatites are characterized by high amounts of calcite, with negligible amounts of magnesium carbonate minerals (e.g., dolomite and ankerite), thus indicating that the Huayangchuan calcite carbonatites are derived from low-degree partial melting of carbonated eclogites.

Although low degree partial melting of carbonated eclogites may be the origin of calcite carbonatite, it seems to present some difficulties in explaining the right-inclined flat distribution patterns [Calcite: $(\text{La}/\text{Yb})_N = 0.9\text{--}4.2$, this study; Carbonatite: $(\text{La}/\text{Yb})_N = 1.97\text{--}4.93$, Xu et al., 2007; $(\text{La}/\text{Yb})_N = 4.89\text{--}22.82$, Xue et al., 2020] with slight LREE enrichment of carbonatite at Huayangchuan. This inevitably requires that the $(\text{La}/\text{Yb})_N$ values or LREE/HREE values of the primary carbonatite melt is equivalent or even lower than this, which is attributed to the fact that the Huayangchuan carbonatite has undergone highly fractionated processes (see Subsection 6.2). Adam and Green (2001) showed that the partition coefficient of LREE in garnet is much lower ($D_{\text{La}} < 0.001$; $D_{\text{Ce}} < 0.009$) than that of HREE ($D_{\text{Yb}} = 7.2$; $D_{\text{Lu}} = 6.2$) in the melting process; in other words, the residual garnet has a great ability to absorb HREE preferentially over LREE and this experimental result can well explain the majority of LREE-rich carbonatites around the world. As a result, it is generally considered that the highly LREE-

Table 2

The results of bulk carbon and oxygen isotopic compositions of multi-type calcites.

Sample type	Rock type	Colour	Calcite type	Mineral	Grain size	$\delta^{13}\text{C}_{\text{VPDB}}$ (‰)	$\delta^{18}\text{O}_{\text{VPDB}}$ (‰)	$\delta^{18}\text{O}_{\text{VSMOW}}$ (‰)
Un-mineralized calcite carbonatites (UMCC)	Quartz calcite carbonatite	White	Cal-I	Calcite	Coarse-grained	-7.07	-23.14	7.05
	Quartz calcite carbonatite	White		Calcite	Coarse-grained	-7.08	-22.54	7.68
	Quartz calcite carbonatite	White		Calcite	Coarse-grained	-7.06	-22.27	7.95
	Quartz calcite carbonatite	White		Calcite	Coarse-grained	-7.09	-22.02	8.21
	Quartz calcite carbonatite	White		Calcite	Medium-grained	-6.90	-23.33	6.86
	Quartz calcite carbonatite	White		Calcite	Medium-grained	-6.79	-21.46	8.78
	Quartz calcite carbonatite	White		Calcite	Medium-grained	-6.77	-22.80	7.40
	Quartz calcite carbonatite	White		Calcite	Medium-grained	-6.90	-22.83	7.37
	Aegirine-augite calcite carbonatite	Black		Calcite	Fine-grained	-7.00	-22.44	7.77
		gray						
	Aegirine-augite calcite carbonatite	Black		Calcite	Fine-grained	-6.96	-21.84	8.40
		gray						
	Aegirine-augite calcite carbonatite	Black		Calcite	Fine-grained	-7.05	-21.97	8.26
		gray						
	Aegirine-augite calcite carbonatite	Black		Calcite	Fine-grained	-7.09	-22.51	7.71
		gray						
U-Nb-REE mineralized calcite carbonatites (MCC)	Aegirine-augite calcite carbonatite	Black	Cal-I	Calcite	Medium-grained	-6.89	-21.97	8.26
		gray						
	Aegirine-augite calcite carbonatite	Black		Calcite	Medium-grained	-6.95	-21.98	8.25
		gray						
	Aegirine-augite calcite carbonatite	Black		Calcite	Medium-grained	-6.87	-22.04	8.19
		gray						
	Aegirine-augite calcite carbonatite	Black		Calcite	Medium-grained	-7.07	-21.99	8.24
		gray						
	Aegirine-augite calcite carbonatite	Black		Calcite	Medium-grained	-6.95	-21.88	8.35
		gray						
	Aegirine-augite calcite carbonatite	Black		Calcite	Medium-grained	-7.03	-22.09	8.13
		gray						
	Barite-bearing aegirine-augite calcite carbonatite	Black		Calcite	Medium- to fine-grained	-6.91	-20.60	9.67
		gray						
	Barite-bearing aegirine-augite calcite carbonatite	Black		Calcite	Medium- to fine-grained	-6.92	-22.05	8.17
		gray						
	Barite-bearing aegirine-augite calcite carbonatite	Black		Calcite	Medium- to fine-grained	-6.89	-21.86	8.37
		gray						
	Barite-bearing aegirine-augite calcite carbonatite	Black		Calcite	Medium- to fine-grained	-6.88	-22.14	8.09
		gray						
	Aegirine-augite calcite carbonatite	Black		Calcite	Fine-grained	-7.11	-21.66	8.59
		gray						
	Aegirine-augite calcite carbonatite	Black		Calcite	Fine-grained	-6.79	-21.20	9.05
		gray						
	Aegirine-augite calcite carbonatite	Black		Calcite	Fine-grained	-6.80	-20.57	9.70
		gray						
Sample type	Rock type	Colour	Calcite type	Mineral	Grain size	$\delta^{13}\text{C}_{\text{VPDB}}$ (‰)	$\delta^{18}\text{O}_{\text{VPDB}}$ (‰)	$\delta^{18}\text{O}_{\text{VSMOW}}$ (‰)
U-Nb-REE mineralized calcite carbonatites (MCC)	Aegirine-augite calcite carbonatite	Black	Cal-I	Calcite	Fine-grained	-6.76	-21.98	8.25
		gray						
	Aegirine-augite calcite carbonatite	Black		Calcite	Fine-grained	-7.13	-21.23	9.02
		gray						
	Aegirine-augite calcite carbonatite	Black		Calcite	Fine-grained	-7.49	-20.87	9.40
		gray						
	Galena-bearing aegirine-augite calcite carbonatite	Black		Calcite	Fine-grained	-7.02	-22.13	8.10
		gray						
	Aegirine-augite calcite carbonatite	Black		Calcite	Fine-grained	-7.01	-21.58	8.66
		gray						
Post-mineralized zeolite calcite veins (PMZV)	Biotite calcite carbonatite	Pink white		Calcite	Medium-grained	-6.82	-21.86	8.37
	Biotite calcite carbonatite	Pink white		Calcite	Fine-grained	-6.86	-21.51	8.74
	Biotite calcite carbonatite	Pink white		Calcite	Fine-grained	-6.84	-22.06	8.17
	Biotite calcite carbonatite	Pink white		Calcite	Fine-grained	-6.79	-22.04	8.19
Post-mineralized zeolite calcite veins (PMZV)	Biotite calcite carbonatite	Pink white		Calcite	Fine-grained	-6.96	-21.86	8.38
	Biotite calcite carbonatite	Pink white		Calcite	Fine-grained	-6.81	-21.95	8.28

(continued on next page)

Table 2 (continued)

Sample type	Rock type	Colour	Calcite type	Mineral	Grain size	$\delta^{13}\text{C}_{\text{VPDB}}$ (‰)	$\delta^{18}\text{O}_{\text{VPDB}}$ (‰)	$\delta^{18}\text{O}_{\text{VSMOW}}$ (‰)
	Zeolite calcite vein	Light brown		Calcite		-10.25	-18.86	11.47
	Zeolite calcite vein	Light brown		Calcite		-9.89	-19.43	10.88
	Zeolite calcite vein	Light brown		Calcite		-10.22	-19.01	11.32
	Zeolite calcite vein	Light brown		Calcite		-10.75	-17.40	12.98
	Zeolite calcite vein	Light brown		Calcite		-10.76	-16.97	13.42
	Gypsum-zeolite calcite vein	Light brown		Calcite		-10.60	-15.29	15.15
	Gypsum-zeolite calcite vein	Light brown		Calcite		-10.62	-15.14	15.30
	Zeolite calcite vein	Light brown		Calcite		-10.82	-16.49	13.91
	Zeolite calcite vein	Light brown		Calcite		-10.92	-16.53	13.87
	Aegirine-augite zeolite calcite vein	Light brown		Calcite		-11.01	-15.95	14.46
	Aegirine-augite zeolite calcite vein	Light brown		Calcite		-10.79	-16.82	13.57
	Aegirine-augite zeolite calcite vein	Light brown		Calcite		-10.60	-16.93	13.46
	Zeolite calcite vein	Light brown		Calcite		-10.60	-16.70	13.69
	Zeolite calcite vein	Light brown		Calcite		-10.71	-16.68	13.72

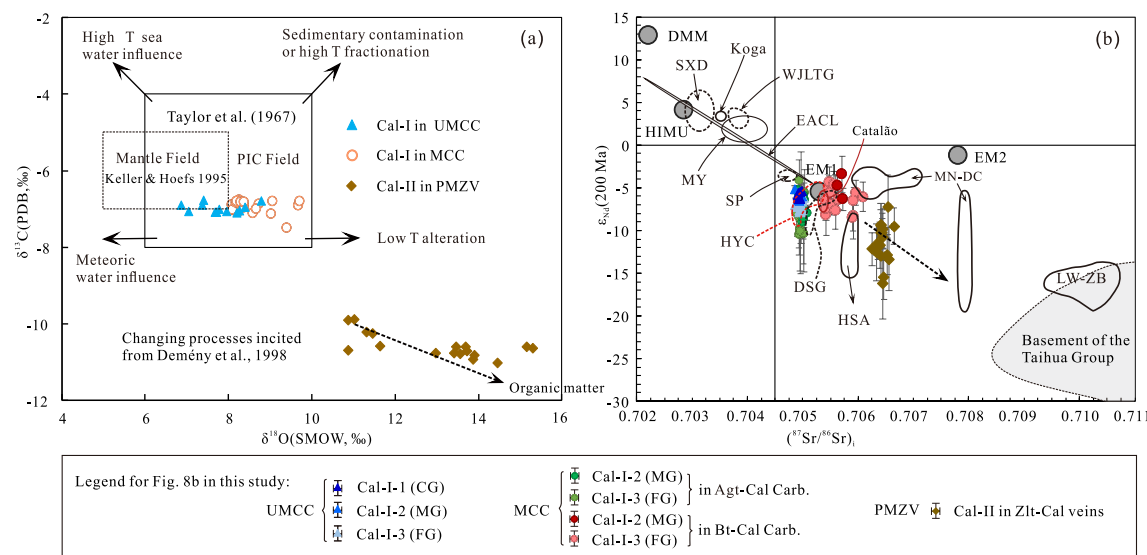


Fig. 8. (a) C and O isotopic compositions of calcites for carbonatitic veins from the Huayangchuan ore district in this study. Primary igneous carbonatite (PIC) field proposed by Taylor et al. (1967) and mantle field is cited from Keller and Hoefs (1995). The processes of the changes in C–O isotopic composition is cited from Demény et al. (1998). (b) In-situ Sr–Nd isotopic compositions for different types of calcites from carbonatites and post-mineralized zeolite–calcite veins at Huayangchuan in this study. The data sources of the Huayangchuan calcite Sr–Nd isotopes are listed in Table A3. The Sr–Nd isotopic compositions of the basements of Taihua Group obtained from Gao et al. (2014). The binary diagram and the end-member components of DMM, EM1, EM2 and HIMU are taken from Zindler and Hart, 1986. Other data sources of carbonatites: HYC (Huayangchuan, NQL, China, Xu et al., 2011); DSG (Dashigou, NQL, China, Xu et al., 2011); HSA (Huangshui'an, NQL, China, Huang et al., 2009); MY (Miaoya, SQL, China, Su et al., 2019); SXD (Shaxiongdong, SQL, China, Xu et al., 2008); MN-DC (Mianning-Dechang, Panxi, China, Xu et al., 2003; Hou et al., 2006); LW-ZB (Laiwu-Zibo, Shandong, China, Ying et al., 2004); WJLTG (Wajilitage, Tarim, China, Cheng et al., 2017); SP (Shilman and Patti, Pakistan, Tilton et al., 1998); Koga, Pakistan, Tilton et al., 1998); Catalão, Brazil, Cordeiro et al., 2010); EACL (East African Carbonatite Line, Bell and Blenkinsop, 1987).

rich carbonatite magma is produced during the low degree partial melting process of carbonated eclogites. Therefore, some researchers have interpreted the Huayangchuan carbonatites as the product of low degree partial melting in the garnet-poor mantle source (Xu et al., 2007) or shallow garnet-poor mantle (Xue et al., 2020). However, this knowledge is derived from limited high-temperature and high-pressure

partitioning experiments for garnet/melt. Westrenen et al. (1999) interestingly showed that the partition coefficient (D) of LREE and HREE between garnet and anhydrous silicate melt (i.e., the starting materials with SiO₂ content from 40.8 to 47.7 wt%) is greatly depend on the Mg/(Mg + Ca) of garnet (i.e. the composition ratio of pyrope (Py) and grossular (Gr)). They found from Py₈₄Gr₁₆ to Py₉Gr₉₁, D_{La} increases

sharply from 0.004 to 0.2, whereas D_{Lu} and D_{Yb} decreases slightly from 5.7 to 2.7 and 3.9 to 2.8, respectively. Unfortunately, to the best of our knowledge, no relevant partition coefficients ($D_{garnet/carbonatite\ melt}$) for variable components of garnet has been reported at present. We first assume that there exists a similar rule in the garnet/carbonatite melt system. With low-degree partial melting of carbonated eclogites (with mode of clinopyroxene ($Cpx_{0.5}$) + garnet ($Grt_{0.5}$)), garnet will be the residual phase, and then, bulk D is calculated based on melt mode ($Cpx_{0.9} + Grt_{0.1}$) of eclogites in this study (See Table A4). As shown in Table A4, bulk D_{La} of Py9Gr91, Py60Gr40 and Py65Gr35 eclogites ($D_{La} = 0.1581\text{--}0.2211$) is significantly higher than that of Py82Gr18 and Py84Gr16 ($D_{La} = 0.0087\text{--}0.0141$), while bulk D_{Yb} is slightly decreased from 3.61 to 2.44. Based on this, different REE distribution patterns of eclogites from the Qinling-Dabie area (Huang et al., 2000; Gu, 2012) were used as the starting materials for simulation (See Table A5). As shown in Table A5, our simulation results show that low degree partial melting ($\leq 1\%$) of the LREE-rich eclogites always produces melt with high $(La/Yb)_N$ values [$(La/Yb)_N = 30\text{--}1559$], but cannot produce melt with low $(La/Yb)_N$ values (1.97–22.82, Xu et al., 2007; Xue et al., 2020). For the HREE-rich eclogites, interestingly, low degree of partial melting of eclogites (Py9Gr91, Py60Gr40 and Py65Gr35) $\leq 1\%$ could produce the primary melt with low $(La/Yb)_N$ values [$(La/Yb)_N = 1.20\text{--}9.16$], which is similar to that of Huayangchuan carbonatite. Therefore, we propose that Huayangchuan HREE-rich carbonatite may be the result of low degree partial melting of HREE-rich patterns carbonated eclogites, but further experimental verification of the partition coefficients between variable components of garnet and carbonatite melt is needed.

6.2. Magmatic evolution and mechanism for ore-forming element enrichment

The Cal-I calcites (both, unmineralized and mineralized carbonatites) display similar trace element characteristics (Fig. 6) and Sr-Nd-C-O isotopic compositions (Fig. 8), indicating their similar EM1 mantle-derived source material. In the binary diagram of $(^{87}\text{Sr}/^{86}\text{Sr})_i$ vs. Sr concentration, except for few altered mineralized samples with relatively high $(^{87}\text{Sr}/^{86}\text{Sr})_i$ values (Fig. 9a), the carbonatites exhibit a fractional crystallization trend with decreased Sr due to crystallization of Sr-rich minerals (e.g., barytocelestite) (Fig. 3b, e and 4d, i). This trend is also consistent in the ε_{Nd} vs. Nd concentration binary diagram (Fig. 9b) with the decrease in Nd ascribed to the crystallization of REE-bearing minerals (e.g., apatite, allanite, monazite, and betafite) (Fig. 3b, c, e, g), auto-metasomatised hydrothermal activity, or both. In addition, our earlier studies suggest that some betafite grains in the deposit underwent hydrothermal alteration during Yanshanian magmatism (Gao

et al., 2019). However, this process did not have significant effects on the calcite Sr isotopic results owing to the high Sr content of calcites. Some measurement results and errors in Nd isotopic values, showing slightly higher values for mineralized and post-mineralized calcites, can be attributed to their relatively low Nd content. Nevertheless, the contamination of post-mineralized Cal-II calcites by crustal organic matter (e.g., graphite-rich Taihua group wall rocks) (Shou, 2018) and the fractional crystallization trend of carbonatite magmas are still significant (Figs. 8 and 9). The Huayangchuan carbonatites are thus inferred to have experienced strong fractional crystallization. In this process, crystallization of early silicate minerals such as aegirine-augite, amphibole, mica and K-feldspar as well as early calcite can promote the late carbonatite magma more enriched with U-Nb-REE ore-forming elements (Fig. 3a, b, e, f and Fig. 4b-c). This strong fractionation of carbonatitic magma not only led to U, Nb, REE, and Ba enrichment in the orthomagmatic hydrothermal stage (Le Bas, 1987; Knudsen, 1989; Cuney, 2014; Cheng et al., 2018) (instead of entering the rock-forming minerals) but was also associated with carbonatite-exsolved fluids rich in F, Cl⁻, SO₄²⁻, PO₄³⁻, and CO₂ ligands migrating Nb, REE, and U, thus altering the surrounding rocks (Currie and Ferguson, 1971; Kresten and Morogan, 1986; Gittins et al., 1990; Bühn and Rankin, 1999; Williams-Jones and Palmer, 2002).

In addition to isotopic signatures, the magmatic evolution process is also recorded by the calcite major and trace element compositions and mineral assemblages. Some studies have shown that the diagrams of Yb/La-Yb/Ca and La/Ho-Y/Ho for calcites can effectively trace the calcite genetic type and magma evolution (Möller et al., 1976; Möller and Morteani, 1983; Bau and Dulski, 1995; Subías and Fernández-Nieto, 1995). Cal-I calcites display gradation from magmatic to magmatic-hydrothermal conditions in the Yb/La-Yb/Ca diagram (Fig. 10a), indicating that carbonatite magmas underwent a continuous evolution from the melt to fluid stage during emplacement process. Melt and fluid inclusion studies of the Maoniuping carbonatite-related REE deposits (Xie et al., 2009) show comparable trends. The calcites (Cal-I-2 and Cal-I-3) from mineralized carbonatites plot into the hydrothermal field (Fig. 10a) and display a core-rim texture (Fig. 3c and 12), accompanied by presence of barytocelestite (Fig. 3b and e), indicating that the U-Nb-REE mineralization mainly occurred in the orthomagmatic hydrothermal stage. For calcites (Cal-I-1, Cal-I-2 and Cal-I-3) from fresh unmineralized carbonatites, the Y/Ho ratios are similar to chondritic magmas (Fig. 10b) implying CHArge-and-RAdius-Controlled (CHARAC) processes (Bau, 1996). It is noteworthy that the LREE content decreases steadily from coarse- to fine-grained samples (Fig. 11a), which may be ascribed to the crystallization of LREE-bearing minerals (such as apatite) (Chakhmouradian et al., 2016; Fig. 4i), but the slightly increasing trend

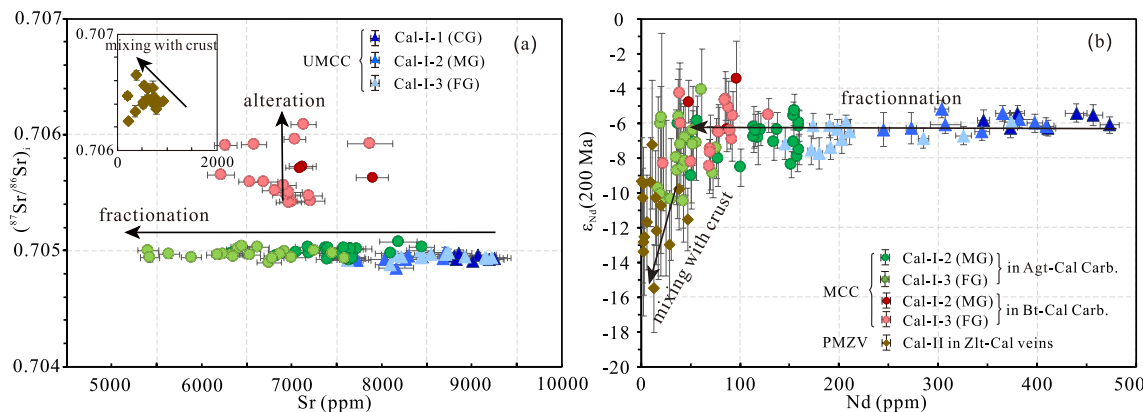


Fig. 9. Binary diagrams showing (a) $(^{87}\text{Sr}/^{86}\text{Sr})_i$ vs. Sr concentration and (b) ε_{Nd} vs. Nd concentration (DePaolo, 1988). The calcite Sr and Nd concentrations decrease with carbonatite evolution reflecting in situ crystal fractionation by Sr-minerals and LREE-minerals, respectively. Cal-II (brown) calcites in post-mineralized zeolite-calcite veins display mixing with crust. Data sources of in situ calcite and Sr-Nd isotopic compositions in this study are listed in Table A3, and the trace elemental (Sr and Nd) data used are from Table A2.

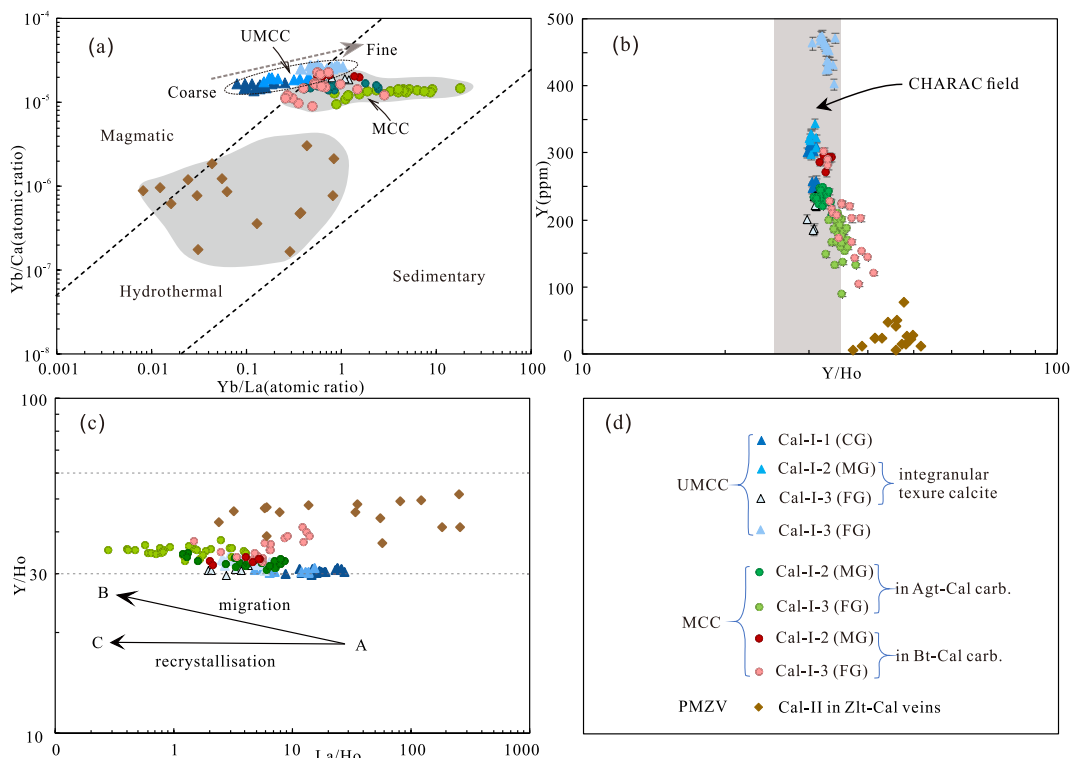


Fig. 10. Plots of (a) Yb/La (atomic ratio) vs. Yb/Ca (atomic ratio) (Möller et al., 1976; Möller and Morteani, 1983), (b) Y/Ho ratio vs. Y concentration (Bau, 1996) and (c) La/Ho ratio vs. Y/Ho ratio (Bau and Dulski, 1995) for different types of calcites from the Huayangchuan U-Nb-REE deposit. (d) Legend for different types of calcites. The CHARAC field of Y/Ho ratios in (b) is defined by Bau (1996). The migration and recrystallisation trends in (c) are taken from Bau and Dulski (1995). The data sources of in situ calcite major and trace elemental compositions for different types of calcites from the Huayangchuan U-Nb-REE deposit in this study are listed in Tables A1 and A2.

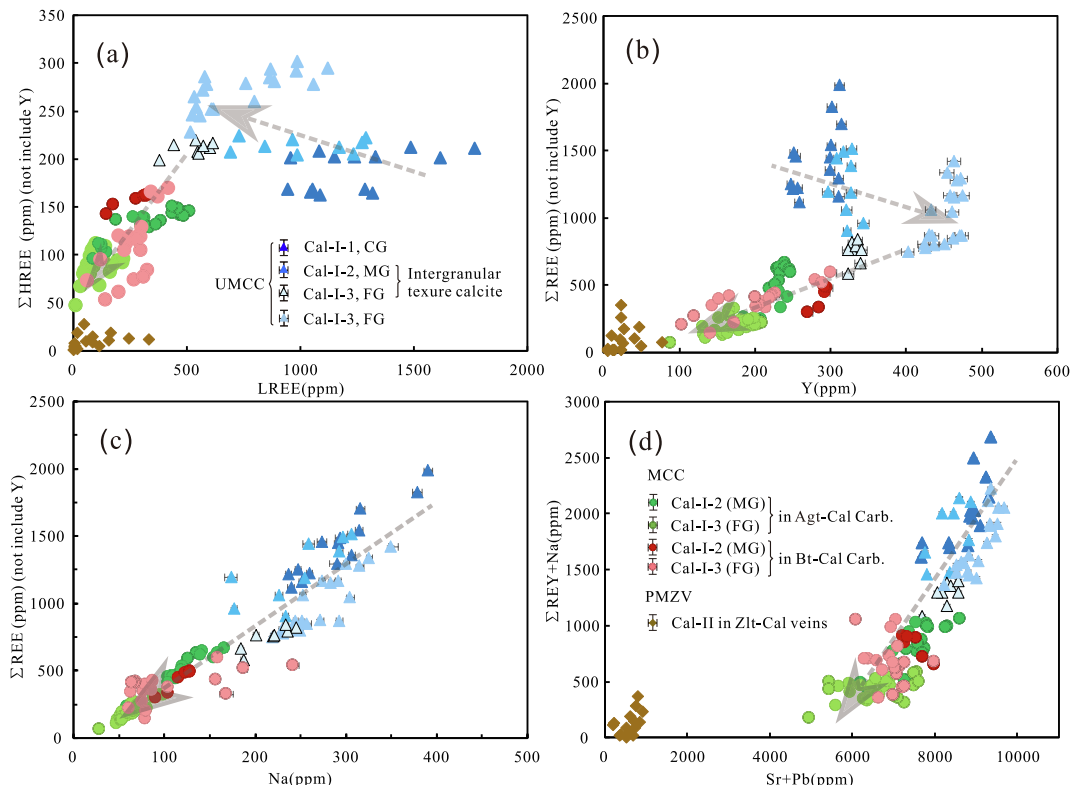
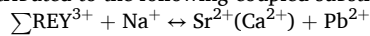


Fig. 11. Trace element (including REE) plots of, (a) LREE-HREE, (b) Y vs. \sum REE, (c) Na vs. \sum REE, and (d) Sr + Pb vs. REY + Na for different types of calcites from the Huayangchuan U-Nb-REE deposit. The direction of arrow represents the trends of change between trace elements. The data sources of in situ calcite trace elemental compositions in this study are listed in Table A2.

of HREE(Y) contents (Fig. 10b and 11a, b) indicates that the preferential crystallization of LREE-bearing minerals may lead to significant differentiation between LREE and HREE in the absence of significant carbonatite-exsolved fluids.

In addition, the good correlation between Na vs. \sum REE and Sr + Pb vs. \sum REY + Na diagrams for Cal-I calcites (Fig. 11c, d) reveals that the dominant mechanism for REE incorporation into calcites may be attributed to the following coupled substitution:



Compared to Cal-I calcites from unmineralized carbonatites, calcites

from mineralized samples (Cal-I-2 and Cal-I-3) show sharp decreasing trend for LREE and HREE(Y) contents (Fig. 11a, b) and relatively lower Na and REE contents (Fig. 11c, d). The decrease in Na and REE contents in the mineralized calcites may be due to the carbonatite-exsolved ore-forming fluids accompanying alkaline fenitization (Fig. 2e, f), and the crystallization of abundant LREE-rich minerals (e.g., monazite-Ce and allanite-Ce; Fig. 3e, g) or LREE-bearing minerals (e.g., apatite and betafite-Ce; Fig. 3b,c) and minor HREY-rich minerals (e.g., samarskite-Y, Fig. 3h) during intense fluid–rock reactions (characterized by intense fenitization and biotitization). It is noted that the igneous calcite (Cal-I)

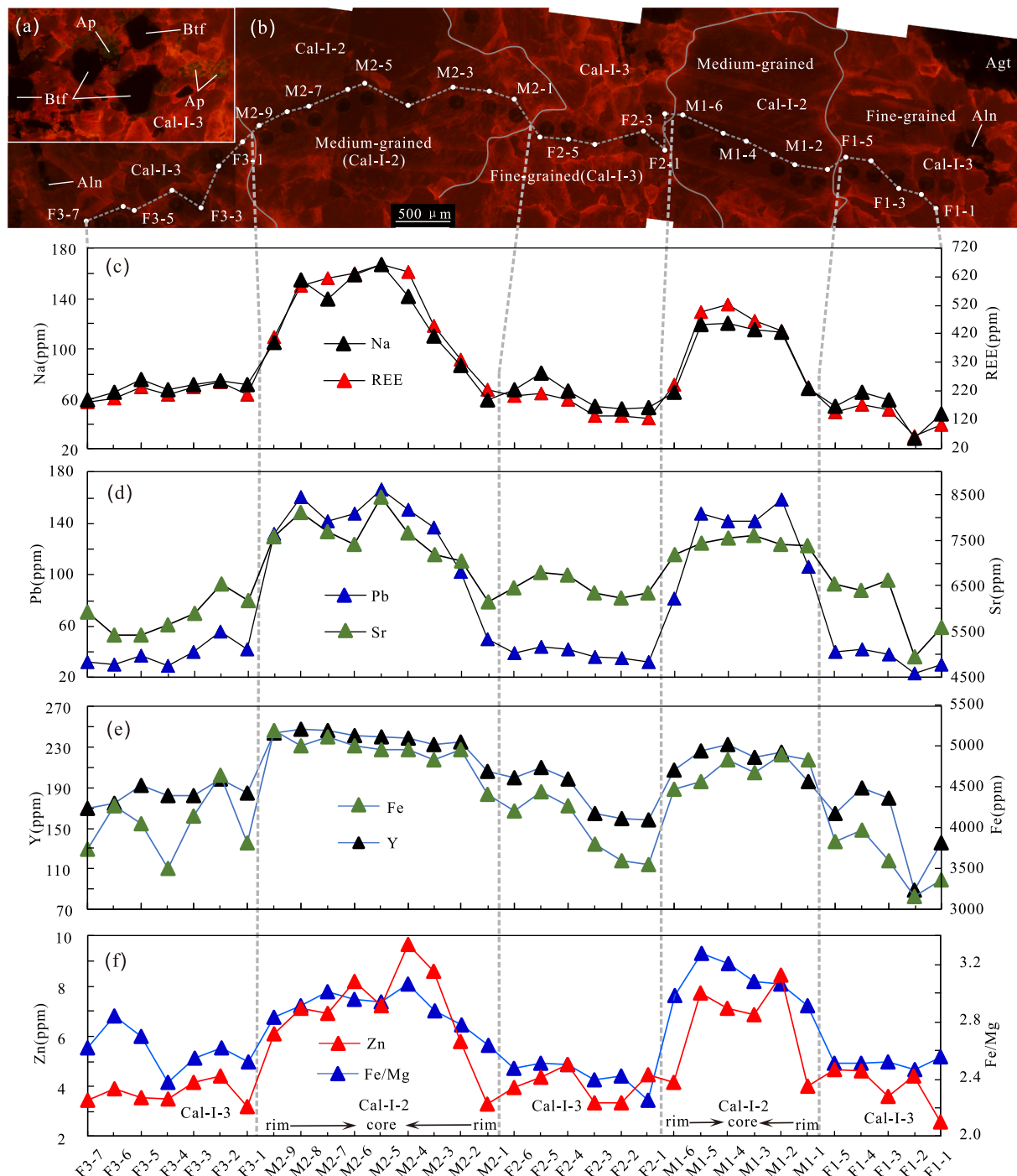


Fig. 12. Core-rim texture of calcite from mineralized aegirine–augite calcite carbonatites and its trace element change tendency profile as determined by LA-ICP-MS. (a) Betafite paragenesis with Cal-I-3 and apatite. (b) Two stage calcites (Cal-I-2 and Cal-I-3) and their test locations. (c–f) Correlation diagrams of Na–REE, Pb–Sr, Y–Fe, Zn–Fe/Mg. The data sources of in situ calcite trace elemental compositions are listed in Table A2.

from the Huayangchuan carbonatite system is characterized by HREY enrichment (136–774 ppm) and the Huayangchuan carbonatite shows a certain degree of HREY mineralization potential, which is also rare in the global carbonatite, except other carbonatites in the NQL. At present, very limited case studies from the Songwe Hill carbonatite (Malawi), indicated that apatite in late hydrothermal stage is characterized by HREY enrichment, which may be ascribe to the different ability of LREE and HREE complexes to migrate stably with hydrothermal fluids (Broom-Fendley et al., 2017). However, unlike the Songwe Hill carbonatite, the whole system of Huayangchuan carbonatite is relatively HREY-rich. As mentioned above in the discussion on the origin of carbonatite, the HREY enrichment in the Huayangchuan carbonatite system may be related to an HREY-rich source and highly evolved processes of carbonatite magma.

Furthermore, calcites from mineralized carbonatites display a certain degree of recrystallization and migration trends in the La/Ho-Y/Ho diagram (Fig. 10c). Mineral chemistry and chronology of betafite and uraninite reveal that the Huayangchuan deposit has been superimposed by fairly hydrothermally metasomatized Yanshanian magmatism at ca. 129 Ma (Gao et al., 2019). Similar calcite Sr-Nd isotopic signatures in mineralized and unmineralized carbonatitic samples support the conclusion that the intense carbonatite-exsolved fluids auto-metasomatized, assimilating parts of calcite REE (Cal-I-2 and Cal-I-3) into hydrothermal fluids, eventually developing core-rim textures in calcites from mineralized carbonatitic samples (Fig. 3c and 12), with the loss of Na, Sr, Pb, Fe, and Zn contents and decrease in Fe/Mg ratio along the rim to the core (Fig. 12c-f). The Cal-I-3 calcites from mineralized aegirine-augite calcite carbonatite occur in paragenesis with betafite, apatite, and allanite, with negligible monazite or other rare earth minerals (Fig. 3b-c and 12a), suggesting that the mechanism of metasomatism for REE removal from calcites (Cal-I-2 and Cal-I-3) in carbonatites may not have played a dominant role in REE mineralization at Huayangchuan, though hydrothermal reworking may have been a significant factor in some other deposits (Gysi and Williams-Jones, 2013; Li and Zhou, 2015; Ying et al., 2020). Few calcite grains from mineralized carbonatites (Cal-I-2 and Cal-I-3) exhibit relatively high detectable U (0.21–1.05 ppm, av. 0.46 ppm, n = 7) and Nb (0.21–1.67 ppm, av. 0.58 ppm, n = 11) contents (Fig. 6 and Table A2) than that (Cal-I-1) in the early carbonatite. This may be due to tiny U-Nb-rich inclusions, implying that these calcite grains may have formed in a U-Nb-rich magmatic-hydrothermal system. Therefore, we suggest that highly differentiated evolution of carbonatite magmas with exsolved ore-forming fluids (residual fluids) may play an important role in the enrichment of U-Nb-REE at the late orthomagmatic-hydrothermal stage. Observations from other carbonatite-related deposits in the world further substantiate this mechanism (Knudsen, 1989; Yang and Le Bas, 2004; Xie et al., 2009; Cuney, 2014; Cheng et al., 2018; Bai et al., 2019; Yang et al., 2019).

6.3. Source(s) of ore-forming materials

In addition to the highly evolved mechanism of carbonatite magmas and extensive carbonatite-exsolved fluids, the source producing the carbonatitic magmas that were relatively rich in ore-forming elements (e.g., U, Nb, and REE), or large amounts of ore-forming elements added by assimilation with wall rock during magma upwelling, are equally important. The bulk C-O isotopic characteristics of carbonatites and the Sr-Nd isotopic and trace element compositions of calcites confirm that the Huayangchuan carbonatites are EM1 mantle-derived without obvious magma mixing or wall rock assimilation. These isotopic evidences indicate the mantle origin of U-Nb-REE ore-forming materials at the Huayangchuan deposit. Experimental results show that the low partition coefficients of U-Nb-REE makes these ore-forming elements preferring to enter the carbonatite melt during low degree partial melting of the carbonated eclogite (Hammouda et al., 2009), which is confirmed by the high enrichment in REE (LREE > HREE)-Nb-(U)-Sr-Ba,

and other incompatible elements (Gittins, 1988). Moreover, carbonatite magma with low density, low viscosity (Dobson et al., 1996) and volatile-rich matter (Keppler, 2003) features make it have high solubility and migrating capacity of REE-Nb-U-P-Sr-Ba and other incompatible elements. Experimental studies have shown that 0.1% of the carbonatitic melt extraction from the deep upper mantle can remove 30–60% of the highly incompatible ore-forming elements (e.g., U and REE) (Dasgupta et al., 2009); however, it seems unlikely that the mantle can directly provide large amounts of ore-forming materials for the Huayangchuan deposit due to the extremely low U, Nb, Σ REE, and Y abundances (0.021, 0.658, 6.87, and 4.30 ppm, respectively) (McDonough and Sun, 1995) in the mantle. Isotopic features reveal that the Huayangchuan carbonatites are characterized by EM1 mantle origin (Fig. 8b), similar to Dashigou, but significantly differ from carbonatites of the southern belt (e.g., Shaxiongdong and Miaoya), and other parts of China (e.g., Wajilitage, Mianning-Dechang, Laiwu-Zibo), except Cata-lao carbonatite (Fig. 8b). Previous studies have shown that the recycling of subducted sediments in the oceanic crust may play an important role in formation of collisional orogeny-related carbonatites (Xu et al., 2003, 2014; Hou et al., 2006; Xue et al., 2020) and oceanic carbonatites (Hoernle et al., 2002). Moreover, Kato et al. (2011) found the enrichment of REY in modern deep-sea mud of the Pacific Ocean. This implies that a large amount of REY-rich sediments could be brought into the mantle by plate subduction, eventually leading to preliminary REE enrichment in the mantle by metasomatism (Hou et al., 2015). Previous numerical simulations of carbonatite systems have shown that the recycling of subducted oceanic crust with a few percent (5%) of ancient pelagic sediments into the deep mantle could generate an enriched mantle with EM1 signature (Hou et al., 2006). Therefore, we suggest that some U-Nb-REE-rich crustal sediments, derived by plate subduction, may be involved in the mantle source region that accomplished the pre-enrichment of Huayangchuan U-Nb-REE ore-forming elements.

Additionally, regional studies show that numerous types of uranium deposits, such as the Lantian hydrothermal uranium deposit (Wang et al., 2013), the Guangshigou intrusion-related uranium deposits (Chen et al., 2019), and the Yuecun carbon-silica mudstone type uranium deposits (Li, 2008) in the North Qinling belt. This indicates that the Qinling belt developed an ancient U-rich stratum which may serve as a uranium source for the deposit as well as the Huayangchuan carbonatites, but further evidences are needed.

6.4. Comprehensive genetic model for the deposit

Recent chronological studies reveal that the Huayangchuan carbonatite-related U-Nb-REE deposits mainly formed in Late Triassic (197–229 Ma) (Gao et al., 2019; Xue et al., 2020; Zheng et al., 2020a), although it also yields a Yanshanian age (~129 Ma) due to the superposition of Yanshanian magmatic activity (Gao et al., 2019). Lead isotopic studies show that the Huayangchuan carbonatite is similar to the basement rocks of the SQL, but is obviously distinct from that of the Precambrian rocks in the NCC (Xu et al., 2011). This indicates that the Huayangchuan carbonatite may be mainly related to the subduction process of the Mian-Lüe oceanic crust to the north during Late Triassic. During the end of Late Triassic, with the subduction of the Mian-Lüe oceanic crust to the north, the tectonic regime of the Lesser Qinling area transitioned from transpression to extension/transstension (Chen and Santosh, 2014; Xu et al., 2014). Accordingly, a possible metallogenetic model developed for the Huayangchuan deposit has been shown in Fig. 13.

In Late Triassic, the Mian-Lüe oceanic crust carrying U-Nb-REE-rich sediments subducted and recycled into the Lesser Qinling, where Huayangchuan is located; low-degree partial melting of the metasomatically enriched mantle eclogites led to preliminary enrichment of ore-forming elements (U-Nb-REE) in carbonatite magmas (Fig. 13a). Carbonatite magma with excellent features of low density, low viscosity (Dobson et al., 1996) and volatile-rich matter

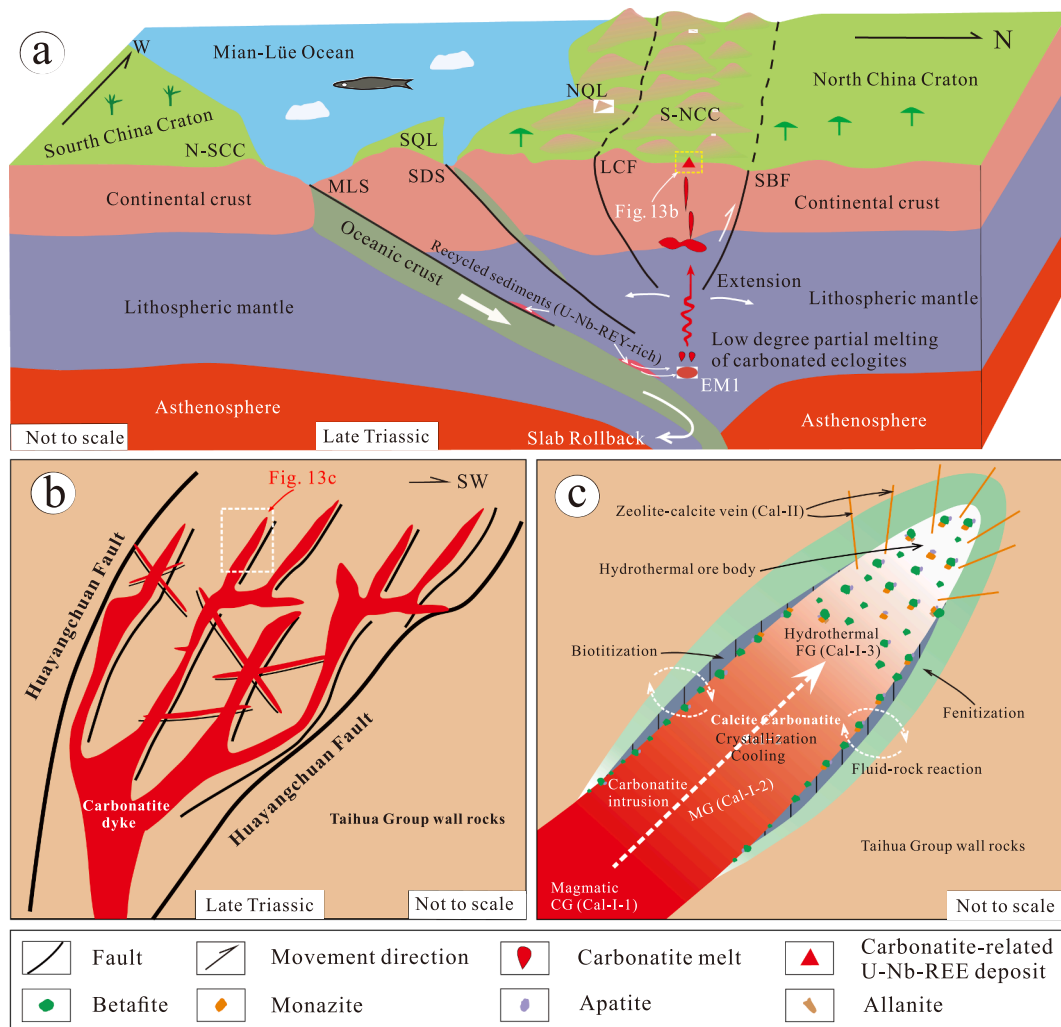


Fig. 13. Formation model of the Huayangchuan deposit. (a) Tectonic background of the Qinling in Late Triassic (modified after Chen and Santosh, 2014). (b) Emplacement morphology and evolution of carbonatites. (c) Carbonatite diagenetic evolution and U–Nb–REE metallogenesis model based on the previous carbonatite models (after Le Bas, 1987; Knudsen, 1989).

(Keppler, 2003) makes it easy to enrich and carry these ore-forming elements (U–Nb–REY) rapidly ascending emplacement. The Huayangchuan carbonatitic magmas then underwent intense magmatic evolution during the intrusive emplacement into the Taihua Group gneiss (Fig. 13b). Intense differentiation caused further enrichment of U–Nb–REE ore-forming elements in the abundant late residual fluids (Knudsen, 1989) and migration in the form of stable complexes (possibly fluorine complexes, sulfate complexes and chlorine complexes) during the late orthomagmatic hydrothermal stage (Fig. 13c). With decreasing concentration of F^- , SO_4^{2-} and PO_4^{3-} away from the intruding carbonatite (Knudsen, 1989; Xue et al., 2020), these stable complexes will be instable. As a result, the cations as U, Nb and REY will be precipitated as betafite–U–Nb, allanite–Ce, monazite–Ce and minor samarskite–Nb–Y. Meanwhile, the process of carbonatite-exsolved fluids and their accompanying auto-metasomatism removed parts of REE into fluids causing the total REE concentration of calcites (Cal-I-2 and Cal-I-3) in mineralized carbonatites to decrease significantly.

Extensive fenitization and biotitization of the contact zones between the mineralized carbonatites and wall rocks (Fig. 2e, f) indicates occurrence of a strong fluid–rock reaction (Fig. 13c). The Huayangchuan U–Nb–REY polymetallic deposits eventually formed owing to the strong material and energy exchange with surrounding rocks. Therefore, we suggest that the unique Huayangchuan carbonatite-related U–Nb–REE polymetallic deposits formed in Late Triassic due to transition in the

tectonic regime from transpression to extension/transtension and as a result of the coupling of the U–Nb–REY–rich recycled sediments, intense magmatic evolution, and extensive fluid–rock reactions.

7. Conclusions

Based on field, petro-mineralogy, major and trace elements, and Sr–Nd–C–O isotopic studies, the following conclusions have been drawn regarding the formation of the Huayangchuan carbonatite-related U–Nb–REY polymetallic deposit:

- (1) At least two principal types (Cal-I and II) of calcites have been identified in the Huayangchuan ore district. Cal-I calcites that can be subdivided into three subtypes (Cal-I-1, Cal-I-2, and Cal-I-3) are characterized by igneous properties with EM1 mantle origin, whereas Cal-II calcites are late hydrothermal origin.
- (2) The Sr–Nd–C–O isotopic data indicates that the Huayangchuan carbonatites could be derived from low-degree partial melting of HREE-rich carbonated eclogites, and the ore-forming materials of the carbonatite-related deposit may be mainly the result of subduction and recycling of U–Nb–REY–rich oceanic crust sediments.
- (3) Crystallization of LREE-bearing minerals resulted in significant differentiation between LREE and HREE prior to extensive exsolution of fluids from carbonatitic magmas. U–Nb–REY

mineralization occurred in the late magmatic-hydrothermal stage owing to extensive exsolution of ore-forming fluids during highly differentiated evolution of U-Nb-REY-rich carbonatitic magma. The fluid-rock reactions led to the instability of the U-Nb-REE complexes, which may have played an important role in the formation of the Huayangchuan U-Nb-REY deposit.

- (4) The Huayangchuan carbonatite-related deposit emplaced due to the transition in tectonic regime from compressional/transpression to extensional/trans-tension owing to the subduction of the Mian-Liie oceanic crust at the end of Late Triassic.

Declaration of Competing Interest

The authors declare that they have no known competing financial interests or personal relationships that could have appeared to influence the work reported in this paper.

Acknowledgements

This research is financially supported by the Strategic Priority Research Program (B) of Chinese Academy of Sciences (Grant No. XDB18030200) and the National Natural Science Foundation of China (Grant Nos. 41473049 and 41103027). Thanks to Dr. Cheng Gao and Qing-Qing Kang senior engineer from the Geological Team 224 Sino Shaanxi Nuclear Industry Group for their help in the field geology work of Huayangchuan. Drs. Jing Gu, Xiang Li and Yan-Wen Tang from the Institute of Geochemistry, Chinese Academy of Sciences are kindly thanked for performing C-O isotopic and in-situ major and trace element analyses for this paper, respectively. Prof. Huan-Zhang Lu (University of Quebec) is greatly appreciated for his constructive suggestions. The authors would also like to thank the Editor, Dr. Xue-Ming Yang (Manitoba Geological Survey) and another anonymous reviewer for their helpful comments and constructive suggestions to have improved the quality of this paper.

Appendix A. Supplementary data

Supplementary data to this article can be found online at <https://doi.org/10.1016/j.oregeorev.2021.104310>.

References

- Adam, J., Green, T., 2001. Experimentally determined partition coefficients for minor and trace elements in peridotite minerals and carbonatitic melt, and their relevance to natural carbonatites. *Eur. J. Mineral.* 13, 815–827.
- Bai, T., Chen, W., Jiang, S.Y., 2019. Evolution of the carbonatite Mo-HREE deposits in the Lesser Qinling Orogen: Insights from *in situ* geochemical investigation of calcite and sulfate. *Ore Geol. Rev.* 113, 103069.
- Bau, M., 1996. Controls on the fractionation of iso-ovalent trace elements in magmatic and aqueous systems: Evidence from Y/Ho, Zr/Hf, and lanthanide tetrad effect. *Contrib. Mineral. Petro.* 123, 323–333.
- Bau, M., Dulski, P., 1995. Comparative study of yttrium and rare-earth element behaviours in fluorine-rich hydrothermal fluids. *Contrib. Mineral. Petro.* 119, 213–223.
- Bell, K., Blenkinsop, J., 1987. Nd and Sr isotopic compositions of East African carbonatites: implications for mantle heterogeneity. *Geology* 15, 99–102.
- Bell, K., Rukhlov, A.S., 2004. Carbonatites from the Kola Alkaline Province: origin, evolution and source characteristics. In: Wall, F., Zaitsev, A.N. (Eds.), *Phoscorites and Carbonatites from Mantle to Mine: the Key Example of the Kola Alkaline Province*. The Mineralogical Society, London, pp. 433–468.
- Blundy, J., Dalton, J., 2000. Experimental comparison of trace element partitioning between clinopyroxene and melt in carbonate and silicate systems, and implications for mantle metasomatism. *Contrib. Mineral. Petro.* 139, 356–371.
- Brooker, R.A., 1998. The effect of CO₂ saturation on immiscibility between silicate and carbonate liquids: an experimental study. *J. Petrol.* 39, 1905–1915.
- Broom-Fendley, S., Brady, A.E., Wall, F., Gunn, G., Dawes, W., 2017. REE minerals at the Songwe Hill carbonatite, Malawi: HREE-enrichment in late-stage apatite. *Ore Geol. Rev.* 81, 23–41.
- Bühn, B., Rankin, A.H., 1999. Composition of natural, volatile-rich Na-Ca-REE-Sr carbonatitic fluids trapped in fluid inclusions. *Geochim. Cosmochim. Acta* 63, 3781–3797.
- Chakhmouradian, A.R., Reguir, E.P., Couëslan, C., Yang, P., 2016. Calcite and dolomite in intrusive carbonatites II. Trace-element variations. *Mineral. Petro.* 110, 361–377.
- Chen, R.L., 2019. Geochemical characteristics of trace elements from the Huayangchuan U-Nb-Pb deposit, Shaanxi, China. MS dissertation, East China University of Technology master dissertation 1–109 (in Chinese with English abstract).
- Chen, W., Simonetti, A., 2013. In-situ determination of major and trace elements in calcite and apatite, and U-Pb ages of apatite from the Oka carbonatite complex: Insights into a complex crystallization history. *Chem. Geol.* 353, 151–172.
- Chen, Y.J., Santosh, M., 2014. Triassic tectonics and mineral systems in the Qinling Orogen, central China. *Geol. J.* 49, 338–358.
- Chen, Y.W., Hu, R.Z., Bi, X.W., Luo, J.C., 2019. Genesis of the Guangshigou pegmatite-type uranium deposit in the North Qinling Orogenic Belt, China. *Ore Geol. Rev.* 115, 103165.
- Cheng, Z.G., Zhang, Z.C., Hou, T., Santosh, M., Chen, L.L., Ke, S., Xu, L.J., 2017. Decoupling of Mg-C and Sr-Nd-O isotopes traces the role of recycled carbon in magnesiocarbonatites from the Tarim Large Igneous Province. *Geochim. Cosmochim. Acta* 202, 159–178.
- Cheng, Z.G., Zhang, Z.C., Aibai, A.K., Kong, W.L., Holtz, F., 2018. The role of magmatic and post-magmatic hydrothermal processes on rare-earth element mineralization: A study of the Bachu carbonatites from the Tarim Large Igneous Province, NW China. *Lithos* 314–315, 71–87.
- Cordeiro, P.F.O., Brod, J.A., Dantas, E.L., Barbosa, E.S.R., 2010. Mineral chemistry, isotope geochemistry and petrogenesis of niobium-rich rocks from the Catalão I carbonatite-phoscorite complex, Central Brazil. *Lithos* 118, 223–237.
- Cuney, M., 2014. Felsic magmatism and uranium deposits. *Bull. Soc. Géol. France* 185, 75–92.
- Currie, K., Ferguson, J., 1971. A study of fenitization around the alkaline carbonatite complex at Callander Bay, Ontario, Canada. *Can. J. Earth Sci.* 8, 498–517.
- Dalton, J.A., Presnall, D.C., 1998. Carbonatitic melts along the solidus of model lherzolite in the system CaO-MgO-Al₂O₃-SiO₂-CO₂ from 3 to 7 GPa. *Contrib. Mineral. Petro.* 131, 123–135.
- Dasgupta, R., Hirschmann, M., Smith, N., 2007. Partial melting experiments of peridotite + CO₂ at 3 GPa and genesis of alkalic ocean island basalts. *J. Petrol.* 48, 2093–2124.
- Dasgupta, R., Hirschmann, M.M., McDonough, W.F., Spiegelman, M., Withers, A.C., 2009. Trace element partitioning between garnet lherzolite and carbonatite at 6.6 and 8.6 GPa with applications to the geochemistry of the mantle and of mantle-derived melts. *Chem. Geol.* 262, 57–77.
- Demény, A., Ahijado, A., Casillas, R., Vennemann, T.W., 1998. Crustal contamination and fluid/rock interaction in the carbonatites of Fuerteventura (Canary Islands, Spain): a C, O, H isotope study. *Lithos* 44, 101–115.
- DePaolo, D.J., 1988. Neodymium isotope geochemistry. Springer-Verlag, Berlin, Heidelberg, pp. 1–187.
- Dobson, D.P., Jones, A.P., Rabe, R., Sekine, T., Kurita, K., Taniguchi, T., Kondo, T., Kato, T., Shimomura, O., Urakawa, S., 1996. In-situ measurement of viscosity and density of carbonate melts at high pressure. *Earth Planet. Sci. Lett.* 143, 207–215.
- Ferguson, J., Currie, K.L., 1971. Evidence of liquid immiscibility in alkaline ultrabasic dikes at Callander Bay, Ontario. *J. Petrol.* 12, 561–585.
- Gao, C., Kang, Q.Q., Jiang, H.J., Zheng, H., Li, P., Zhang, X.M., Li, L., Dong, Q.Q., Ye, X.C., Hu, X.J., 2017. A unique uranium polymetallic deposit discovered in the Qinling orogenic belt: The Huayangchuan super-large U-Nb-Pb-REE deposit associated with pegmatites and carbonatites. *Geochimica* 46, 446–455 (in Chinese with English abstract).
- Gao, L.G., Chen, Y.W., Bi, X.W., Hu, R.Z., Gao, C., Dong, S.H., Luo, J.C., 2019. Chronology and mineral chemistry of the uranium minerals in Huayangchuan uranium-niobium deposit, Shaanxi Province and its implications for uranium mineralization. *Acta Geol. Sin.* 93, 2273–2291 (in Chinese with English abstract).
- Gao, X.Y., Zhao, T.P., Chen, W.T., 2014. Petrogenesis of the early Cretaceous Funishan granites on the southern margin of the North China Craton: Implications for the Mesozoic geological evolution. *J. Asian Earth. Sci.* 94, 28–44.
- Ghosh, S., Ohtani, E., Litasov, K.D., Terasaki, H., 2009. Solidus of carbonated peridotite from 10 to 20 GPa and origin of magnesiocarbonatite melt in the Earth's deep mantle. *Chem. Geol.* 262, 17–28.
- Gittins, J., 1988. The origin of carbonatites. *Nature (news and views)* 335, 295–296.
- Gittins, J., Beckett, M.F., Jago, B.C., 1990. Composition of the fluid phase accompanying carbonatite magma: A critical examination. *Am. Miner.* 75, 1106–1109.
- Gu, X.F., 2012. Petrologic geochemistry and isotopic geochronology of the Luotian eclogites from the North Dabie complex zone, central China. In: University of Science and Technology of China Doctoral thesis, pp. 1–165.
- Gysi, A.P., Williams-Jones, A.E., 2013. Hydrothermal mobilization of pegmatite-hosted REE and Zr at Strange Lake, Canada: A reaction path model. *Geochim. Cosmochim. Acta* 122, 324–352.
- Hamilton, D.L., Freestone, I.C., Dawson, J.B., Donaldson, C.H., 1979. Origin of carbonatites by liquid immiscibility. *Nature* 279, 52–54.
- Hammouda, T., Moine, B.N., Devidal, J.L., Vincent, C., 2009. Trace element partitioning during partial melting of carbonated eclogites. *Phys. Earth Planet. Interiors* 174, 60–69.
- Harmer, R.E., Gittins, J., 1998. The case for primary, mantle-derived carbonatite magma. *J. Petrol.* 39, 1895–1903.
- He, S., Li, Z.Y., Hui, X.C., Guo, J., 2016. ⁴⁰Ar/³⁹Ar geochronology of biotite in Huayangchuan uranium-polymetallic deposit in Shanxi Province and its geological significance. *Uranium Geol.* 32, 159–164 (in Chinese with English abstract).
- Hodell, D.A., et al., 1990. Variation in the strontium isotopic composition of seawater (8 Ma to present): Implications for chemical weathering rates and dissolved fluxes to the oceans. *Chem. Geol.* 80 (4), 291–307.
- Hoernle, K., Tilton, G., Le Bas, M.J., Duggen, S., Garbe-Schönberg, D., 2002. Geochemistry of oceanic carbonatites compared with continental carbonatites: mantle recycling of oceanic crustal carbonate. *Contrib. Mineral. Petro.* 142, 520–542.

- Hou, Z.Q., Tian, S.H., Yuan, Z.X., Xie, Y.L., Yin, S.P., Yi, L.S., Fei, H.Q., Yang, Z.M., 2006. The Himalayan collision zone carbonatites in western Sichuan, SW China: Petrogenesis, mantle source and tectonic implication. *Earth. Planet. Sci. Lett.* 244, 234–250.
- Hou, Z.Q., Liu, Y., Tian, S.H., Yang, Z.M., Xie, Y.L., 2015. Formation of carbonatite-related giant rare-earth-element deposits by the recycling of marine sediments. *Sci. Rep.* 5, 10231.
- Huang, D.H., Hou, Z.Q., Yang, Z.M., Li, Z.Q., Xu, D.X., 2009. Geological and geochemical characteristics, metallogenetic mechanism and tectonic setting of carbonatite vein-type Mo (Pb) deposits in the East Qinling molybdenum ore belt. *Acta Geol. Sin.* 83, 1968–1984 (in Chinese with English abstract).
- Huang, D.H., Wang, Y.C., Nie, F.J., Jiang, X.J., 1985. A new type of molybdenum deposit-geological characteristics and metallogenetic mechanism of the Huanglongpu carbonatite vein-type of molybdenum (lead) deposit, Shaaxi. *Acta Geol. Sin.* 59, 241–257 (in Chinese with English abstract).
- Huang, Z.L., Liu, C.Q., Hu, Y.G., Zhu, J.M., Xiao, H.Y., Xu, C., 2000. Rare-earth element geochemistry of eclogites from the ultra-high pressure metamorphic belt in central China. *Chin. J. Geochem.* 19, 35–44.
- Hui, X.C., Cai, Y.Q., He, S., Feng, Z.S., 2017. Petrologic and geochemical characteristics of carbonatites in Huayangchuan U-Nb-Pb deposit, Shaanxi Province. *Geoscience* 31, 246–257 (in Chinese with English abstract).
- IAEA, 2009. World distribution of uranium deposits (UDEPO) with uranium deposit classification. In: IAEA-TECDOC-1629, pp. 1–117.
- Ionov, D., Harmer, R.E., 2002. Trace element distribution in calcite-dolomite carbonatites from Spitskop: inferences for differentiation of carbonatite magmas and the origin of carbonates in mantle xenoliths. *Earth Planet. Sci. Lett.* 198, 495–510.
- Isnard, H., Brennetot, R., Caussignac, C., Caussignac, N., Chartier, F., 2005. Investigations for determination of Gd and Sm isotopic compositions in spent nuclear fuels samples by MC-ICPMS. *Int. J. Mass Spectrom.* 246, 66–73.
- Jacques, A.L., 2008. Australian carbonatites: Their resources and geodynamic setting. In: 9th International Kimberlite Conference extended abstract extended Abstract, pp. 1–3.
- Kamenetsky, V.S., Yaxley, G.M., 2015. Carbonate-silicate liquid immiscibility in the mantle propels kimberlite magma ascent. *Geochim. Cosmochim. Acta* 158, 48–56.
- Kang, Q.Q., Jiang, H.J., Li, P., Zhang, X.M., Dong, Q.Q., Ye, X.C., Gao, C., Zhang, T., Xue, C.C., 2018. Ore mineralogical characteristics of the Huayangchuan U-Nb-Pb deposit. *J. East. China Univ. Technol.* 41, 111–123 (in Chinese with English abstract).
- Kato, Y., Fujinaga, K., Nakamura, K., Takaya, Y., Kitamura, K., Ohta, J., Toda, R., Nakashima, T., Iwamori, H., 2011. Deep-sea mud in the Pacific Ocean as a potential resource for rare-earth elements. *Nat. Geosci.* 4, 535–539.
- Keller, J., Hoefs, J., 1995. Stable isotope characteristics of recent natrocarbonatites from Oldoinyo Lengai. In: Bell, K., Keller, J. (Eds.), Carbonatite Volcanism: Oldoinyo Lengai and the Petrogenesis of Natrocarbonatites. Springer-Verlag, Berlin, Heidelberg, pp. 113–123.
- Keppeler, H., 2003. Water solubility in carbonatite melts. *Am. Miner.* 88, 1822–1824.
- Kjærsgaard, B.A., Hamilton, D.L., Peterson, T.D., 1995. Peralkaline nephelinite/carbonatite liquid immiscibility: Comparison of phase compositions in experiments and natural lavas from Oldoinyo Lengai. In: Bell, K., Keller, J. (Eds.), Carbonatite Volcanism: Oldoinyo Lengai and the Petrogenesis of Natrocarbonatites. Springer-Verlag, Berlin, Heidelberg, pp. 163–190.
- Knudsen, C., 1989. Pyrochlore group minerals from the Qaqarsuk carbonatite complex, in: Möller, P., Černý, P., Saupé, F. (eds.), Lanthanides, Tantalum and Niobium. Springer-Verlag, Berlin, Heidelberg, SGA Mineral Deposits Spec. Publ. 7, 80–99.
- Kresten, P., Morogan, V., 1986. Fenitization at the Fen complex, Southern-Norway. *Lithos* 19, 27–42.
- Le Bas, M.J., 1987. Nephelinites and carbonatites. *Geol. Soc. London. Spec. Publ.* 30, 53–83.
- Lee, W., Wyllie, P.J., 1996. Liquid immiscibility in the join $\text{NaAlSi}_3\text{O}_8-\text{CaCO}_3$ to 2.5 GPa and the origin of calciocarbonatite magmas. *J. Petrol.* 37, 1125–1152.
- Li, J.H., 2008. The geological characteristics of carbonate-siliceous-argillitic type uranium ore deposits in Henan. *J. East China Univ. Technol.* 31, 121–126 (in Chinese with English abstract).
- Li, S., 1982. Geochemical features and petrogenesis of Miaoya carbonatites, Hubei Province. *Geochemistry (Engl. Edn.)* 1, 409–420.
- Li, X.C., Zhou, M.F., 2015. Multiple stages of hydrothermal REE remobilization recorded in fluorapatite in the Paleoproterozoic Yinachang Fe-Cu-(REE) deposit Southwest China. *Geochim. Cosmochim. Acta* 166, 53–73.
- McDonough, W.F., Sun, S.S., 1995. The composition of the Earth. *Chem. Geol.* 120, 223–253.
- Meng, Q.R., Zhang, G.W., 1999. Timing of collision of the North and South China blocks: Controversy and reconciliation. *Geology* 27, 123–126.
- Meng, Q.R., Zhang, G.W., 2000. Geologic framework and tectonic evolution of the Qinling orogen, central China. *Tectonophysics* 323, 183–196.
- Möller, P., Parekh, P.P., Schneider, H.J., 1976. The application of $\text{Tb}/\text{Ca}-\text{Tb}/\text{La}$ abundance ratios to problems of fluorspar genesis. *Miner. Depos.* 11, 111–116.
- Möller, P., Morteani, G., 1983. On the geochemical fractionation of rare earth elements during the formation of Ca-minerals and its application to problems of the genesis of ore deposits. In: Augustithis, S.S. (Ed.), The Significance of Trace Elements in Solving Petrogenetic Problems and Controversies. Theophrastus, Athens, pp. 747–791.
- Nelson, D.R., Chivas, A.R., Chappell, B.W., McCulloch, M.T., 1988. Geochemical and isotopic systematics in carbonatites and implications for the evolution of ocean-island sources. *Geochim. Cosmochim. Acta* 52, 1–17.
- Qiu, J.X., Zeng, G.C., Li, C.N., 1993. Alkaline igneous rocks in Qinling-Daba Mountains. *Geol. Publ. House, Beijing*, 1–183 (in Chinese).
- Ramos, F.C., Wolff, J.A., Tollstrup, D.L., 2004. Measuring $^{87}\text{Sr}/^{86}\text{Sr}$ variations in minerals and groundmass from basalts using LA-MC-ICPMS. *Chem. Geol.* 211, 135–158.
- Sage, R.P., 1987. Geology of carbonatite-alkalic rock complexes in Ontario: James Bay Lowlands, districts of Cochrane and Kenora. *Ontario Geological Survey, Study 42*, 49.
- Shou, L., 2018. Metallogenetic characteristics and mineralization zoning of granite deposits in Shaanxi Province. *Northwestern Geol.* 51, 185–191 (in Chinese with English abstract).
- Su, J.H., Zhao, X.F., Li, X.C., Hu, W., Chen, M., Xiong, Y.L., 2019. Geological and geochemical characteristics of the Miaoya syenite-carbonatite complex, Central China: Implications for the origin of REE-Nb-enriched carbonatite. *Ore Geol. Rev.* 113, 103101.
- Subías, I., Fernández-Nieto, C., 1995. Hydrothermal events in the Valle de Tena (Spanish Western Pyrenees) as evidenced by fluid inclusions and trace-element distribution from fluorite deposits. *Chem. Geol.* 124, 267–282.
- Sun, S.S., McDonough, W.F., 1989. Chemical and isotopic systematics of oceanic basalts: Implications for mantle composition and processes. *Geological Society, London, Special Publications* 42, 313–345.
- Tarbuck, E.J., Lutgens, F.K., 2017. Earth: An introduction to physical geology, 12th Edition. Pearson Education Limited, England, pp. 1–816.
- Taylor, H.P., Frechen, J., Degens, E.T., 1967. Oxygen and carbon isotope studies of carbonatites from the Laacher See District, West Germany and the Alnö District Sweden. *Geochim. Cosmochim. Acta* 31, 407–430.
- Tilton, G.R., Bryce, J.G., Mateen, A., 1998. Pb-Sr-Nd isotope data from 30 and 300 Ma collision zone carbonatites in Northwest Pakistan. *J. Petrol.* 39, 1865–1874.
- USGS, 2020. Mineral commodity summaries 2020: U.S. Geological Survey, 1–200.
- Veksler, I.V., Nielsen, T.F.D., Sokolov, S.V., 1998a. Mineralogy of crystallized melt inclusions from Gardiner and Kovdor ultramafic alkaline complexes: Implications for carbonatite genesis. *J. Petrol.* 39, 2015–2031.
- Veksler, I.V., Petibon, C., Jenner, G.A., Dorfman, A.M., Dingwell, D.B., 1998b. Trace element partitioning in immiscible silicate-carbonate liquid systems: An initial experimental study using a centrifuge autoclave. *J. Petrol.* 39, 2095–2104.
- Verhulst, A., Balaganskaya, E., Kirnarsky, Y., Demaiffe, D., 2000. Petrological and geochemical (trace elements and Sr-Nd isotopes) characteristics of the Paleozoic Kovdor ultramafic, alkaline and carbonatite intrusion (Kola Peninsula, NW Russia). *Lithos* 51, 1–25.
- Verwoerd, W.J., 1986. Mineral deposits associated with carbonatites and alkaline rocks. In: Anhaeusser, C.R., Maske, S. (Eds.), Mineral Deposits of Southern Africa 1–2. Geological Society of South Africa, Johannesburg, pp. 2173–2191.
- Wang, J.B., Li, W.H., Lai, S.C., 2013. Discussion on ore-control factors and mineralization of the lantian uranium field Shaanxi. *Northwestern Geol.* 46, 154–161 (in Chinese with English abstract).
- Weng, Z.H., Jowitt, S.M., Mudd, G.M., Haque, N., 2015. A detailed assessment of global rare earth element resources: Opportunities and challenges. *Econ. Geol.* 110, 1925–1952.
- Westrenen, W.V., Blundy, J., Wood, B., 1999. Crystal-chemical controls on trace element partitioning between garnet and anhydrous silicate melt. *Am. Miner.* 84, 838–847.
- Williams-Jones, A.E., Palmer, D.A.S., 2002. The evolution of aqueous-carbonic fluids in the Amba Dongar carbonatite, India: Implications for fenitisation. *Chem. Geol.* 185, 283–301.
- Woolley, A.R., 1987. Alkaline rocks and carbonatites of the World. Part 1: North and South America. British Museum (Natural History), London, pp. 1–216.
- Xie, Y.L., Hou, Z.Q., Yin, S.P., Dominy, S.C., Xu, J.H., Tian, S.H., Xu, W.Y., 2009. Continuous carbonatitic melt-fluid evolution of a REE mineralization system: Evidence from inclusions in the Maoniuping REE Deposit, Western Sichuan, China. *Ore Geol. Rev.* 36, 90–105.
- Xu, C., Huang, Z., Liu, C., Qi, L., Li, W., Guan, T., 2003. Geochemistry of carbonatites in Maoniuping REE deposit, Sichuan province, China. *Sci. China Earth Sci.* 46, 246–256.
- Xu, C., Campbell, I.H., Allen, C.M., Huang, Z., Qi, L., Zhang, H., Zhang, G., 2007. Flat rare earth element patterns as an indicator of cumulate processes in the Lesser Qinling carbonatites, China. *Lithos* 95, 267–278.
- Xu, C., Campbell, I.H., Allen, C.M., Chen, Y., Huang, Z., Qi, L., Zhang, G., Yan, Z., 2008. U-Pb zircon age, geochemical and isotopic characteristics of carbonatite and syenite complexes from the Shaxiongdong, China. *Lithos* 105, 118–128.
- Xu, C., Taylor, R.N., Kynicky, J., Chakhmouradian, A.R., Song, W., Wang, L., 2011. The origin of enriched mantle beneath North China block: Evidence from young carbonatites. *Lithos* 127, 1–9.
- Xu, C., Chakhmouradian, A.R., Taylor, R.N., Kynicky, J., Li, W., Song, W., Fletcher, I.R., 2014. Origin of carbonatites in the South Qinling orogen: Implications for crustal recycling and timing of collision between the South and North China Blocks. *Geochim. Cosmochim. Acta* 143, 189–206.
- Xue, S., Ling, M.X., Liu, Y.L., Kang, Q.Q., Huang, R.F., Zhang, Z.K., Sun, W.D., 2020. The formation of the giant Huayangchuan U-Nb deposit associated with carbonatite in the Qinling Orogenic Belt. *Ore Geol. Rev.* 122, 103498.
- Yang, K.F., Fan, H.R., Pirajno, F., Li, X.C., 2019. The Bayan Obo (China) giant REE accumulation conundrum elucidated by intense magmatic differentiation of carbonatite. *Geology* 47, 1198–1202.
- Yang, X.M., Le Bas, M.J., 2004. Chemical compositions of carbonate minerals from Bayan Obo, Inner Mongolia, China: Implications for petrogenesis. *Lithos* 72, 97–116.
- Yang, Y.H., Wu, F.Y., Wilde, S.A., Liu, X.M., Zhang, Y.B., Xie, L.W., Yang, J.H., 2009. In situ perovskite Sr-Nd isotopic constraints on the petrogenesis of the Ordovician Mengyin kimberlites in the North China Craton. *Chem. Geol.* 264, 24–42.
- Yang, Y.H., Wu, F.Y., Yang, J.H., Chew, D.M., Xie, L.W., Chu, Z.Y., Zhang, Y.B., Huang, C., 2014. Sr and Nd isotopic compositions of apatite reference materials used in U-Th-Pb geochronology. *Chem. Geol.* 385, 35–55.

- Ying, J.F., Zhou, X.H., Zhang, H.F., 2004. Geochemical and isotopic investigation of the Laiwu-Zibo carbonatites from western Shandong Province, China, and implications for their petrogenesis and enriched mantle source. *Lithos* 75, 413–426.
- Ying, Y.C., Chen, W., Simonetti, A., Jiang, S.Y., Zhao, K.D., 2020. Significance of hydrothermal reworking for REE mineralization associated with carbonatite: Constraints from in situ trace element and C-Sr isotope study of calcite and apatite from the Miaoya carbonatite complex (China). *Geochim. Cosmochim. Acta* 280, 340–359.
- Yu, X.H., 1992. Geological, mineralogical characteristics and origin of the carbonatites from Huayangchuan, Shanxi Province. *Earth Sci. (J. China Univ. Geosci.)* 17, 151–158+244 (in Chinese with English abstract).
- Zhang, G., Dong, Y., Lai, S., Guo, A., Meng, Q., Liu, S., Cheng, S., Yao, A., Zhang, Z., Pei, X., Li, S., 2004. Mianlue tectonic zone and Mianlue suture zone on southern margin of Qinling-Dabie orogenic belt. *Sci. China Earth Sci.* 47, 300–316.
- Zhang, W., Chen, W.T., Gao, J.F., Chen, H.K., Li, J.H., 2019. Two episodes of REE mineralization in the Qinling Orogenic Belt, Central China: in-situ U-Th-Pb dating of bastnäsite and monazite. *Miner. Depos.* 54, 1265–1280.
- Zheng, H., Chen, H., Li, D., Wu, C., Chen, X., Lai, C.K., 2020a. Timing of carbonatite-hosted U-polymetallic mineralization in the supergiant Huayangchuan deposit, Qinling Orogen: Constraints from titanite U-Pb and molybdenite Re-Os dating. *Geosci. Front.* 11, 1581–1592.
- Zheng, H., Chen, H.Y., Wu, C., Jiang, H.J., Gao, C., Kang, Q.Q., Yang, C.S., Wang, D.Q., Lai, C.K., 2020b. Genesis of the supergiant Huayangchuan carbonatite-hosted uranium-polymetallic deposit in the Qinling Orogen, Central China. *Gondwana Res.* 86, 250–265.
- Zindler, A., Hart, S., 1986. Chemical geodynamics. *Annu. Rev. Earth Planet. Sci.* 14, 493–571.